UNIVERSITY OF CHEMICAL TECHNOLOGY AND METALLURGY

FACULTY OF CHEMICAL TECHNOLOGY

DEPARTMENT OF TEXTILE, LEATHER AND FUELS

Assist. Prof. Eng. Georgi Bozhilov Georgiev

Synthesis and Application of Modified Carbon Materials Derived from Renewable Raw Materials and Industrial Wastes

DISSERTATION ABSTRACT

presented for the acquisition of the Educational and scientific degree "Doctor"

Professional field: 5.10. Chemical Technology
Speciality „Technology of natural and synthetic fuels"

Scientific Supervisors: Assoc. Prof. Eng. Vesislava Toteva, PhD
Prof. Boyko Tsynstarski, PhD

Scientific committee:
1. ……. - committee chair
2. ……. - reviewer
3. ……. - reviewer
4. …….
5. …….

Sofia, 2026

The dissertation consists of 120 pages and includes 46 figures and 27 tables. A total of 141 sources are cited.

The submitted dissertation was discussed and approved for defense at a meeting of the extended scientific council of the academic unit of the Department of Textile, Leather and Fuels, held on 15 April 2026.

The public defense of the dissertation will be held on ..... at ..... in room ....., building "....." of UCTM.

The materials are available to interested parties on the UCTM website and in the Department of Scientific Activities, room 406, 4th floor, building "A" of UCTM.

Introduction and problem significance

Under contemporary conditions of increasing scarcity of natural resources, intensifying environmental constraints, and the need to reduce the carbon footprint, the development of sustainable carbon materials has become a key scientific and technological challenge.

In recent years (2023–2026), particular emphasis has been placed on implementing the strategies of the European Green Deal and the transition toward a circular economy, in which waste streams are regarded as a valuable resource for producing high value-added materials.

The main scientific problem is associated with the limited development of efficient methods for obtaining functionalized carbon materials from renewable and waste feedstocks, enabling precise control over pore structure, surface chemistry, and consequently over their performance characteristics.

The relevance of the study arises from the need to develop sustainable, low-cost, and multifunctional carbon materials through targeted utilization of biogenic and industrial wastes. This is in direct alignment with the principles of the circular economy, industrial decarbonization, and the trend toward replacing fossil-based materials with renewable alternatives.

Based on the identified scientific problem and the contemporary requirements for sustainable carbon materials, the present research focuses on the development, modification, and application of materials with controlled structure and surface properties.

The aim of the present dissertation is to obtain modified carbon materials from renewable raw materials and industrial wastes, and to investigate their structure, surface chemistry, and functional properties with regard to their application as adsorbents for wastewater treatment and as catalysts in chemical processes.

To achieve the objective of the dissertation, the following tasks are defined:

1. **Selection, investigation, and characterization of renewable raw materials and wastes** (lignocellulosic biomass, industrial, municipal, and construction wastes) in order to assess their potential for producing efficient adsorbents.
2. **Synthesis and modification of carbon materials** through the application of conventional and modified methods (pyrolysis, chemical and physical activation, functionalization), and determination of the optimal conditions required to achieve the target properties.

3. **Physicochemical characterization of the obtained materials** using modern instrumental techniques to determine their textural parameters and surface chemistry.

4. **Evaluation of the applicability of the carbon materials** as adsorbents for water purification and as catalysts, through investigation of their adsorption and catalytic performance.

Conclusions from the literature review

1. Renewable lignocellulosic raw materials and various industrial wastes are promising precursors for obtaining carbon materials with well-developed porous structures and high added value.
2. The type and composition of the initial feedstock are decisive for structure formation during carbonization and for the potential development of micro-, meso-, and macroporous structures, which necessitates preliminary characterization and targeted selection of suitable precursors.
3. The synthesis method (pyrolysis, physical or chemical activation) and the technological parameters of the process are critical for determining the textural characteristics and surface chemistry of the resulting materials.
4. Targeted chemical modification enables the introduction of functional groups and active sites that govern the adsorption capacity and catalytic activity of carbon materials.
5. Modern instrumental techniques allow the establishment of relationships between structure, surface chemistry, and the functional properties of carbon materials.
6. Literature data confirm the potential of modified carbon materials for both wastewater treatment and catalytic processes; however, there remains a need for an integrated approach combining feedstock selection, optimized synthesis, detailed characterization, and evaluation of their applicability.

In this context, the present dissertation is relevant from both scientific and practical perspectives, as it focuses on the production and investigation of modified carbon materials derived from renewable and waste feedstocks with potential applications in environmental and chemical-technological processes.

EXPERIMENTAL SECTION

2.1. Materials used

To achieve the objectives of the dissertation, various samples of activated carbons and carbon foams were prepared. As raw materials, biomasses of different origins were used, including wastes from nuts and seeds (almond shells, jojoba pulp and husks, pistachio pulp), fruit residues (orange peels, banana peels), and plant-derived by-products (cocoa husks, algae – a residue from biodiesel production). In addition, RDF (Refuse-Derived Fuel) was used, representing a mixture of highly combustible materials such as paper and plastics.

2.1.1. Waste biomass of plant origin

Table 2 presents the technical analysis of the initial waste biomasses: almond shells, jojoba pulp, jojoba husks, pistachio pulp, orange peels, and banana peels.

Table 2. Technical analysis of precursors for the production of activated carbons

Raw material	Moisture content W, wt%	Volatile matter content V, wt%	Ash content A, wt%
jojoba pulp	0.27	98,64	1.082
pistachio pulp	0.39	98.66	0.942
banana peels	1.36	93.03	5.61
cocoa husks	0.95	95.26	3.78
orange peels	3.8	93.90	2.29
almond shells	0.3	72.91	1.36

2.1.2. Extracted algae

Green algae of the *Chlorophyta* phylum were extracted for the purpose of obtaining oils for biodiesel production.

Table 3. Composition of algae – elemental and technical analysis

Sample	Elemental analysis, wt%					Technical analysis, wt%	
	C	H	N	S	O	Moisture	Ash
Extracted algae, Chlorophyte strain (EA)	27.54	3.54	3.51	1.1	34.54	4.5	38.7
Carbonized extracted algae	21.86	2.41	2.39	1.15	-	-	-

The results of the proximate and elemental analyses show that the algal biomass has a high ash content and a low carbon content.

The algal precursor was examined by thermogravimetric and differential thermal analysis. The results of the thermogravimetric (TG) and differential thermogravimetric (DTG) analyses are presented in Fig. 9.

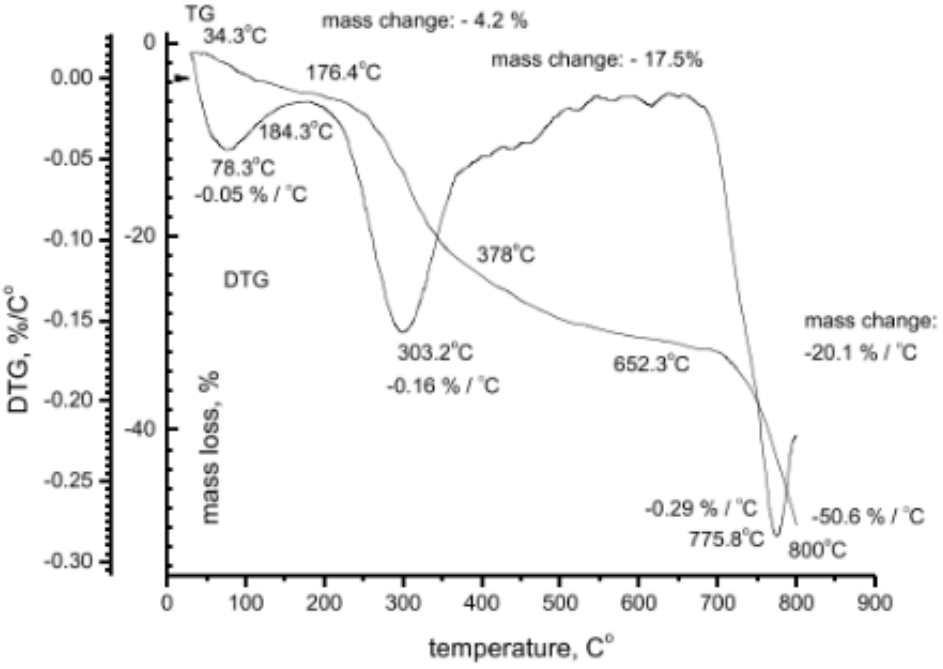

Fig. 9. TG and DTG analysis of extracted algae

The experimental data clearly indicate the presence of three stages of thermal degradation: dehydration (Stage I), condensation (Stage II), and final decomposition (Stage III).

The temperature of maximum decomposition (Tm), observed on the DTG curve during the second stage, is 303 °C. It can be seen that approximately 50% of the sample undergoes thermal transformations up to around 800 °C. The carbon residue accounts for about 20% of the sample.

2.1.3. Bitumen waterproofing material

The accumulation of waste from bitumen waterproofing materials (BWM) represents a serious environmental problem. Table 4 presents the proximate analysis of the BWM sample used as a precursor for obtaining a carbon material.

Table 4. Technical analysis of bitumen waterproofing material

Moisture content W, wt%	Volatile matter content V, wt%	Ash content A, wt%
0.5	69,5	30

2.1.4. Coal tar pitch and furfural

A mixture of commercial coal tar pitch with a softening point of 72 °C and furfural was used as a precursor for obtaining another type of carbon material – carbon foam.

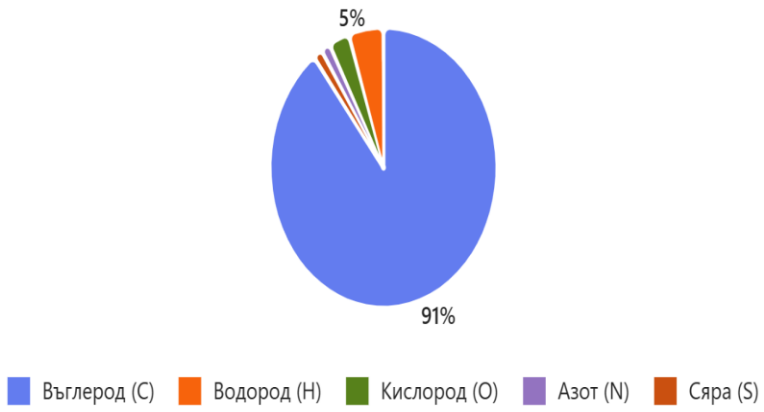

Fig. 10. Elemental composition of the investigated coal tar pitch

The data in Fig. 10 show that the coal tar pitch has a high carbon content, with a C/H ratio of 1.60. The carbon-to-hydrogen ratio is an indicator of the degree of aromatization and polycondensation, which makes this material suitable for carbonization and for producing activated carbon or carbon composites.

2.1.5. Waste polystyrene

Due to its widespread use in food packaging and construction, significant quantities of waste polystyrene are generated. Packaging waste is typically low-density and contains organic

contaminants, whereas construction waste is more homogeneous but often includes impurities from other materials. These characteristics influence the possibilities for recycling and reuse.

Table 5. Technical analysis of waste polystyrene packaging

Moisture content W, wt%	Volatile matter content V, wt%	Ash content A, wt%
0.1	99,5	0,4

2.2. Methods for the preparation of activated carbons

2.2.1. Hydropyrolysis (HPZ)

In this method (HPZ), carbonization and activation occur simultaneously in the presence of water vapor. The raw materials are processed in a stainless-steel reactor placed inside a tubular furnace and heated over a wide temperature range (typically 600–950 °C) at a controlled heating rate and residence time, depending on the specific experimental conditions. The process is carried out in a flow of water vapor, which serves both as a reaction medium and as an activating agent. The samples were pyrolyzed in the presence of water vapor using the apparatus shown in Fig. 11.

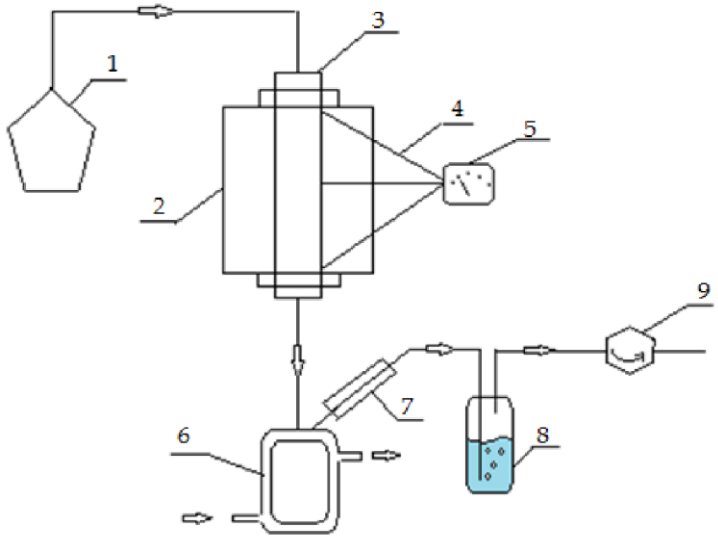

Fig. 11. Hydropyrolysis apparatus (1 – steam generator, 2 – furnace, 3 – reactor, 4 – thermocouples, 5 – temperature controller, 6 – receiver, 7 – condenser, 8 – Drechsel bottle, 9 – gas meter)

2.2.2. Two-stage process for the preparation of activated carbons

To evaluate the efficiency of hydropyrolysis, a two-stage process consisting of carbonization followed by activation was carried out. The raw material was carbonized by heating in a laboratory installation (Fig. 13) at a heating rate of 8 °C/min up to a carbonization

temperature of 500 °C. The sample was held at the final temperature for 10 min and then cooled to room temperature. The solid product was activated with water vapor at 700 °C for 1 h.

To compare steam activation with chemical activation using KOH and phosphoric acid, experiments were performed with jojoba shells. The sample was mixed with the activating agent for 2 h at 60 °C. The resulting suspension was dried at 110 °C in an oven overnight. The dried mixture was then carbonized (sample APc). A second sample was activated by impregnation in a 50% phosphoric acid solution overnight at room temperature (APa).

Table 6. Designations of the obtained samples

Raw material	Single-stage process	Two-stage process
jojoba shells	Carbon A1	Carbon A2
jojoba pulp	Carbon B1	Carbon B2
pistachio pulp	Carbon C1	Carbon C2

2.2.3. Method for the preparation of activated carbons from banana peels, orange peels, and cocoa husks

The fruit-biomass materials were crushed, dried, and subjected to carbonization at 500 °C. Additional chemical activation was performed using KOH and K_2CO_3, followed by carbonization in the range of 550–800 °C. Furthermore, biochars were synthesized either by hydropyrolysis or by CO_2 activation at temperatures between 550 and 750 °C and for different durations (1–3 h).

2.2.4. Preparation of activated carbon from algae

Green algae of the Chlorophyta phylum, previously extracted for oil recovery for biodiesel production, were subjected to pyrolysis at 550 °C with a heating rate of 5 °C/min under an inert atmosphere in the apparatus shown in Fig. 13. The temperature was selected based on the DTG analysis (Fig. 9), which indicates maximum mass loss in the range of 300–400 °C. This suggests that the degradation processes and the formation of activated carbon, which occur simultaneously, are completed at approximately 500–550 °C.

2.2.5. Methods for the preparation of activated carbon from almond shells and for catalyst synthesis

The precursor was subjected to hydropyrolysis (simultaneous carbonization and activation) at 700 °C for 1 h, with a heating rate of 5 °C/min and a water-steam flow rate of 10 cm^3/min (Fig. 11). The resulting activated carbon was ground and sieved to a particle size below 0.4 mm, after which the material was washed with distilled water and dried for 10 h at 110 °C.

Surface modification of the carbon was carried out by treatment with zinc and sulfuric acid. To generate Lewis acidic sites, the carbonized and activated material was impregnated with zinc dissolved in nitric acid, in an amount corresponding to 10 wt%. Brønsted acidic sites were obtained by treating the carbon material with concentrated sulfuric acid (18 M).

2.2.6. Method for the carbonization of bitumen waterproofing material

The bitumen waterproofing material, cut into small squares, was subjected to thermal oxidation in a stirred reactor at 250–300 °C for 30 min, using concentrated H_2SO_4 as the oxidizing agent.

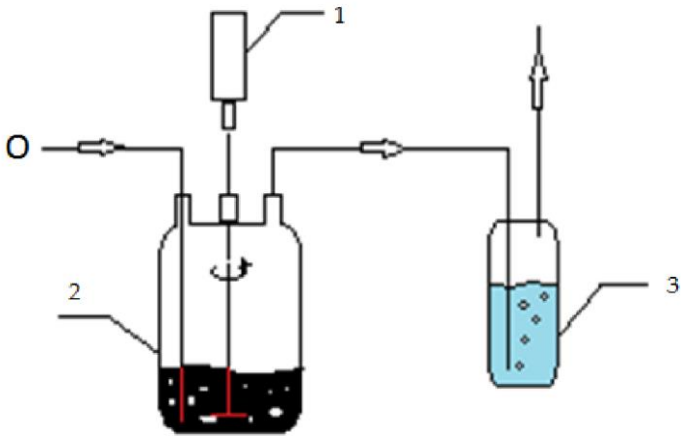

Fig. 12. Scheme of the thermal oxidation process (1 – mechanical stirrer, 2 – stainless-steel reactor, 3 – Drechsel bottle)

The next stage involves thermal treatment in an autogenous atmosphere formed by the volatile products released from the precursor. The oxidized RDF was introduced into a reactor and subjected to heating at 600 °C for 1 h in a furnace (Fig. 13).

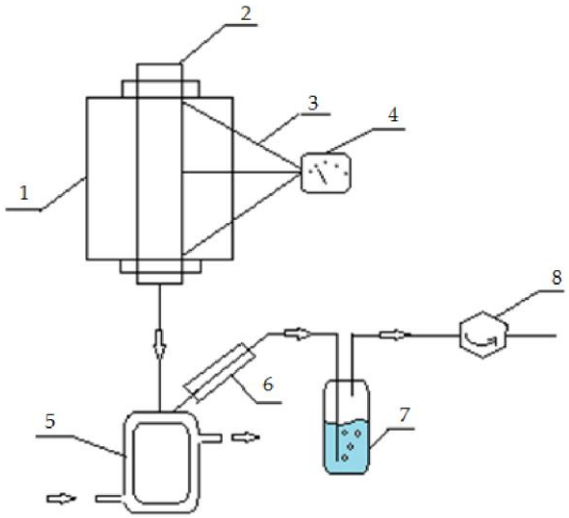

Fig. 13. Thermal treatment (1 – furnace, 2 – reactor, 3 – thermocouples, 4 – temperature controller, 5 – receiver, 6 – condenser, 7 – Drechsel bottle, 8 – gas meter)

The third stage represents hydropyrolysis and is carried out in the apparatus shown in Fig. 11. As a result of the process, new pores are formed and existing ones are widened, leading to the development of a micro-/mesoporous structure.

2.2.7. Method for the carbonization of polystyrene waste

The thermochemical treatment (pyrolysis) of the waste material – polystyrene packaging– was carried out using a procedure analogous to that applied for the treatment of bitumen waterproofing material. In the first stage, the waste material was melted and subjected to oxidation with concentrated sulfuric acid at a weight ratio of 1:1, at 350 °C and under continuous stirring, until a solid product was obtained. In the second stage, the resulting material was pyrolyzed at 900 °C in a carbon dioxide atmosphere, with a heating rate of 10 °C/min.

2.2.8. Method for the preparation of carbon foam

A new method has been developed for the synthesis of carbon foam from a mixture of coal tar pitch and furfural, enabling foam formation without the use of high pressure or a stabilization step. Suitable conditions were established for thermo-oxidative modification with concentrated H_2SO_4 or concentrated HNO_3 of mixtures of furfural and coal tar pitch in various proportions (30–70%), allowing the formation of a porous structure in the resulting carbon foam.

As a result of thermal treatment in the presence of strong acids, the oxygen in the furan ring becomes protonated and the aromaticity is disrupted, leading to the polymerization of furfural.

Synthesis stages

First stage: The coal tar pitch is heated to 110 °C until melted. Furfural is heated to the same temperature and added to the pitch under continuous stirring. The resulting mixture is treated with concentrated H_2SO_4 (98%) or concentrated HNO_3 (63 wt%), with the acid added under continuous stirring until foaming and solidification occur.

Second stage: The solid product is heated to 1000 °C in a covered silicon crucible at a heating rate of 15 °C/min under a nitrogen atmosphere.

RESULTS AND DISCUSSION

3.1. Physicochemical and textural characteristics of carbonized and activated materials obtained from plant biomass

Table 7 presents the relationship between the precursors used, the resulting porous structure, and the specific surface area of the carbons.

Table 7. Precursors used for the preparation of carbon material

precursor	designation	Yeld %	S, BET m^2	Vt cm^3/g	V_{micro} cm^3	V_{meso} cm^3
jojoba pulp	B1	15,8	641	———	———	———
pistachio pulp	C1	10,2	579	———	———	———
banana peels	BC-BP	24,8	910	0,47	0,37	0,05
cocoa husks	BC-CH	18,2	703	0,1	0,22	0,1
orange peels	BC-OP	25,6	421	0,17	0,11	0,05
almond shells	AC	28,3	452	0,22	0,149	0,072
alge	AC1	25	501	0,23	0,15	0,13
bitumen waterpr	RDF	45,4	713	0,12	0,097	0,019
coal tar	CFS	31,6	855	0,464	0,256	0,108
polystyrene	AB X	35	1382	1,025	0,424	0,284

Figure 14 shows the precursors used for the preparation of carbon materials and their application in the adsorption of pollutants from aqueous solutions and in catalytic processes.

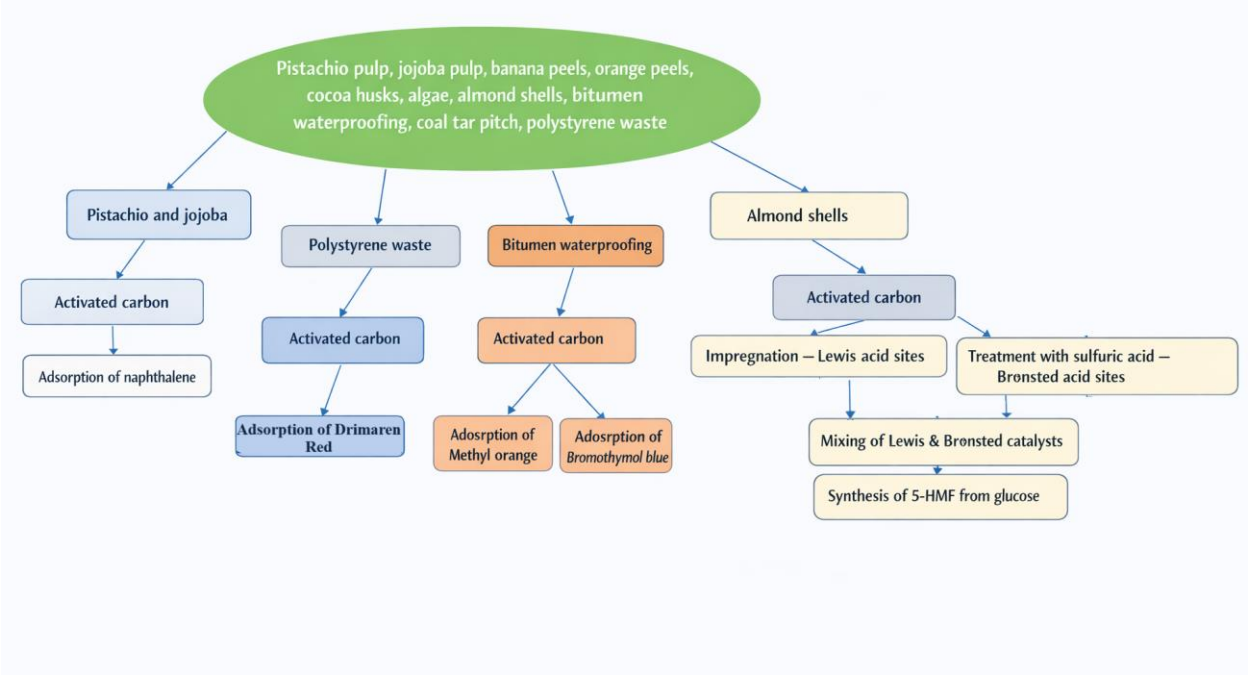

Fig. 14. Overview of raw precursors and the investigated applications of selected carbon materials

3.1.1. Determination of the iodine numbers of activated carbons from jojoba and pistachio

Table 8 presents the iodine numbers, which provide initial information about the specific surface area and the yield of activated carbon obtained from different sources and produced by various activation methods.

Table 8. Iodine numbers and yields of activated carbons obtained from jojoba and pistachio

Activation method	Sample designation	Iodine number, mgJ/g	Yield, %
Jojoba husk, single-stage	A1	621,6	16,0
Jojoba husk, two-stage	A2	619,7	16,7
Jojoba husk, KOH	APc	575,1	17,6
Jojoba husk, H_3PO_4	APa	837,6	17,6
Jojoba pulp, single-stage	B1	641,1	15,8
Jojoba pulp, two-stage	B2	559,9	18,1
Pistachio pulp, single-stage	C1	579.0	10,2
Pistachio pulp, two-stage	C2	573,6	--

Considering the significant amounts of water required for washing during chemical activation, as well as the high energy consumption associated with the two-stage process, the

single-stage method in the presence of water vapor can be regarded as a more economically efficient approach for obtaining activated carbons from jojoba shells.

Furthermore, the results demonstrated that the single-stage pyrolysis method in the presence of water vapor exhibits better performance in terms of textural parameters compared to the two-stage process for the preparation of activated carbon.

3.1.2. Elemental analysis of the activated carbons obtained from jojoba and pistachio

The elemental analysis of the precursors and the activated carbons obtained by steam pyrolysis is presented in Table 9.

Table 9. Elemental analysis of the precursors and the activated carbons obtained by steam activation.

Samples	**C (wt%)**	**H (wt%)**	**N (wt%)**	**S (wt%)**
Jojoba husks	50,23	6,07	1,21	0,18
A1	68,55	2,80	0,77	0,61
APa	72,79	2,46	1,14	0,49
Jojoba pulp	52,71	7,89	3,73	0,38
B1	74,7	1,40	2,82	0,11
Pistachio pulp	41,37	5,25	1,95	0,52
C1	36,73	2,29	0,52	8,30

In the activated carbons (Table 9) obtained from different sources, the carbon content increases. As expected, the hydrogen content decreases relative to carbon after carbonization.

The activated carbon produced from jojoba shells by chemical activation with phosphoric acid exhibits a higher iodine number, higher carbon content, lower oxygen content, and only negligible sulfur content compared to activated carbons obtained from various sources through the single-stage steam-assisted pyrolysis method. It was found that after activation, both the carbon content and the iodine number increase.

3.1.3. Investigation of the surface functional groups of samples APa, A1, B1, and C1

The content of the surface functional groups of the activated carbons, which plays an essential role in their adsorption properties, is presented in Table 10.

Table 10. Neutralization capacity of activated carbon, meq g^{-1}

Activated carbon	Acidic functional groups				Basic functional groups
	Carboxylic groups	Lactones	Hydroxyl groups	Carbonyl groups	
APa	0,10	0,12	1,00	2,00	BDL
A1	BDL	BDL	0,70	1,30	3,30
B1	BDL	BDL	0,83	1,65	1,95
C1	BDL	BDL	BDL	1,58	1,06

BDL – value below the analytical detection limit.

In Table 10, the quantities of the different oxygen-containing groups on the surface of the activated carbons are compared. The data in the table illustrate the influence of the raw materials and the activation method on the nature of the oxygen-containing surface groups. It was established that various oxygen-containing functional groups with different chemical properties are present on the surface of the activated carbon.

3.1.4. Application of activated carbons (APa, A1, B1, C1) from jojoba and pistachio for the removal of naphthalene from water

The adsorption studies of naphthalene from aqueous solutions onto the carbon adsorbents were carried out at ambient temperature in a batch-stirred system. Based on previous investigations of activated carbons derived from different types of biomass, it has been established that adsorption equilibrium is reached after 30 min; therefore, in our experiments the contact time for the different naphthalene concentrations was set to 1 h. The analyses were performed by mixing 50 mL portions of naphthalene solution in a series of conical flasks with 100 mg of adsorbent. After 1 h, the contents of the flasks were filtered through a microporous filter, and the naphthalene concentration was determined spectrophotometrically using a UV spectrometer Pfaro300 at a wavelength of 269 nm.

A kinetic study was conducted, and a Langmuir isotherm was constructed using initial naphthalene concentrations of 1, 10, 20, and 30 mg L^{-1}, with an adsorbent mass of 100 mg per 50 mL solution. The adsorption capacity of the investigated activated carbons was analyzed using the linear form of the Langmuir isotherm model as follows:

$$C_e/q_e = 1/q_m b + C_e/q_m$$

Table 11. Adsorption capacity of activated carbon toward naphthalene

Samples	Adsorption capacity, mg/g	Langmuir adsorption constant, b (L/mg)	R^2
APa	23,8	1,0	0,9978
A1	20,8	5,0	0,9105
B1	22,2	4,0	0,9000
C1	22,0	4,3	0,9423

The correlation coefficients (Table 11), calculated from the Langmuir isotherms using linear regression procedures, show good agreement with the experimental data. This further confirms that the removal of naphthalene from solution by the prepared activated carbons can be described by the Langmuir isotherm, i.e., the adsorption proceeds through monolayer formation, exhibiting the typical L-type behavior according to the Giles classification.

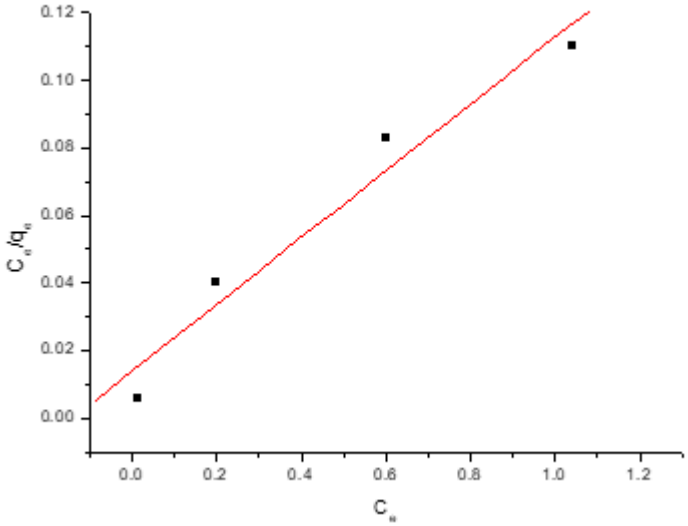

Fig. 15. Langmuir adsorption plot for naphthalene

The activated carbon produced by phosphoric-acid activation (APa) possesses the most developed porous structure (as indicated by its high iodine number) and exhibits the highest adsorption capacity for naphthalene, 23.8 mg g^{-1}, compared to the steam-activated carbon derived from jojoba shells. Among the steam-activated samples, the activated carbon B1 obtained from jojoba pulp shows the highest adsorption capacity, consistent with its highest iodine number relative to the other steam-activated carbons. The activated carbon A1, which has an iodine number 25% lower, demonstrates an adsorption capacity approximately 13% lower than that of APa.

It should also be noted that despite its lower iodine number, sample C1 exhibits a higher adsorption capacity than sample A1, which is evidently due to differences in surface chemistry—specifically, the higher content of carbonyl groups in C1 compared to A1. Mattson et al. (1969) proposed that aromatic compounds are adsorbed onto carbon surfaces through a donor–acceptor complex mechanism, in which the carbonyl oxygen on the carbon surface acts as an electron donor, while the aromatic ring of the adsorbate acts as an electron acceptor. This mechanism is particularly relevant for sample C1, which contains 18% more carbonyl groups and has an iodine number 7% lower than A1, yet exhibits a 5% higher adsorption capacity.

Overall, adsorption can occur at different active sites, and it strongly depends on both the surface chemistry and the iodine number of the activated carbons.

3.1.5. Characterization of the activated carbons obtained from banana peels, orange peels, and cocoa husks

The elemental composition of the activated carbons produced from banana peels, orange peels, and cocoa husks was investigated. The results are presented in Table 12.

Table 12. Moisture content, ash content, and elemental analysis of activated carbons derived from orange peels (BC-OP), cocoa husks (CH), and banana peels (BC-BP)

Sample **wt (%)**	W^a %	A^d %	**C (%)**	**H (%)**	**N (%)**	**S (%)**	**O (%)**
BC-OP	2.04	11.0	79.05	4.11	1.23	0.03	15.58
BC-CH	1.8	13.1	84.7	1.3	1.6	0.3	12.1
BC-BP	1.7	2.6	78	2.5	1.1	0.5	17.9

In Table 13, the adsorption–textural parameters of the obtained activated carbon samples were determined by low-temperature nitrogen adsorption at 77 K.

Table 13. Adsorption–textural parameters of the activated carbon samples derived from orange peels (BC-OP), cocoa husks (CH), and banana peels (BC-BP).

Sample	Iodine number, mg g^{-1}	S_{BET} m^2g^{-1}	V_{total}, cm^3g^{-1}	V_{micro}, cm^3g^{-1}	V_{meso}, cm^3g^{-1}
BC-OP	421	400	0.17	0.11	0.05
BC-CH	703	675	0.35	0.22	0.10
BC-BP	910	820	0.47	0.37	0.05

The pore structure and the main textural parameters of the samples are presented in Figs. 16–20. The presence of hysteresis also confirms the existence of a significant amount of mesopores in the tested sample. This observation is further supported by the pore size distribution obtained using the DFT method (Fig. 19).

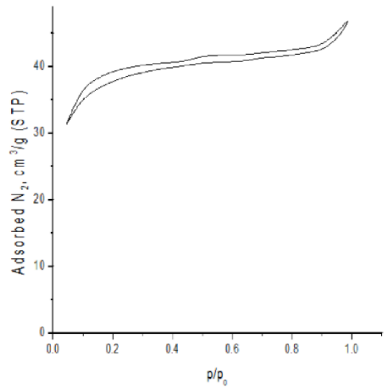

Fig. 16. Nitrogen adsorption isotherm at 77 K of activated carbon derived from orange peels

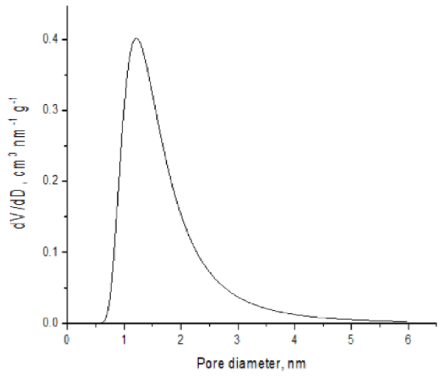

Fig. 17. Pore size distribution of activated carbon derived from orange peels.

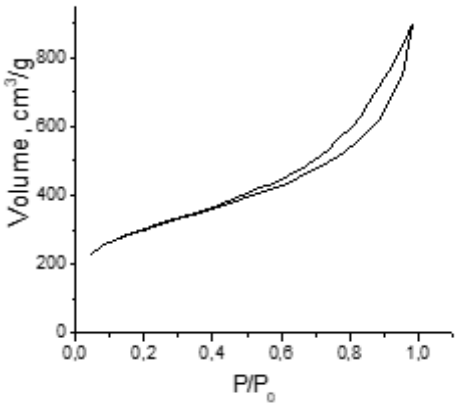

Fig. 18. Nitrogen adsorption isotherm at 77 K of activated carbon derived from cocoa husks.

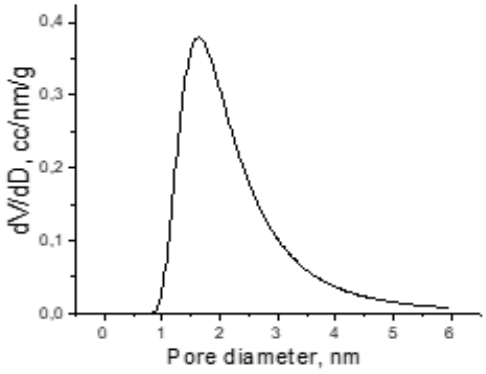

Fig. 19. Pore size distribution of activated carbon derived from cocoa husks.

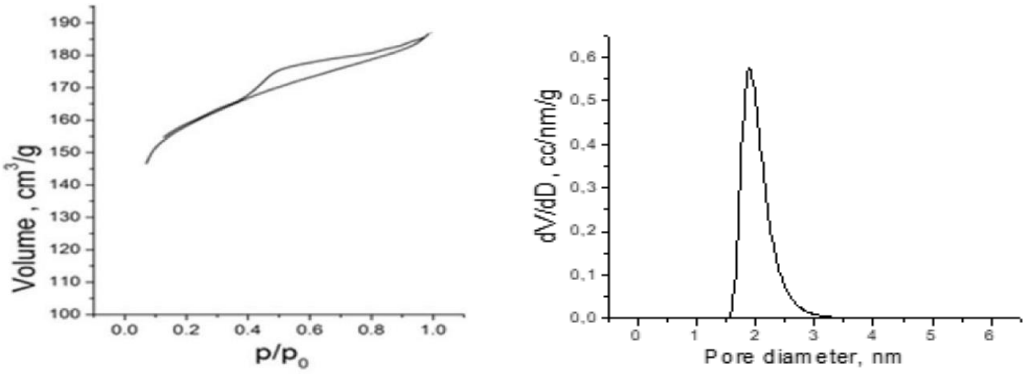

a) b)

Fig. 20. (a) Nitrogen adsorption isotherm at 77 K and (b) pore size distribution of activated carbon derived from banana peels

It was established that the thermochemical conversion of lignocellulosic biomass (banana peels, orange peels, and cocoa husks) enables the production of biochar, as well as liquid intermediates suitable for biofuels and biochemicals.

3.1.6. Characterization of the activated carbon obtained from extracted algae (EA)

The raw material and the resulting carbonized product were analyzed in order to determine their elemental composition and technical characteristics, including moisture and ash content.

Table 14. Elemental and proximate analysis of EA

Sample	Elemental analysis, wt%					Technical analysis wt%	
	C	H	N	S	O	Moisture, W%	Ash, A
Raw material	57.31	3.54	3.51	1.10	34.54	5.50	18.70
Activated carbon from algae	71.88	2.17	2.32	1.32	22.31	5.40	23.80

The pore structure of the carbonized material (AC1) and of the activated sample (AC2), obtained at the previously determined optimal activation temperature, was examined by low-temperature nitrogen physisorption at 77 K. The main textural parameters of the samples are presented in Fig. 21 and Table 14. The specific surface area was calculated using the DFT method.

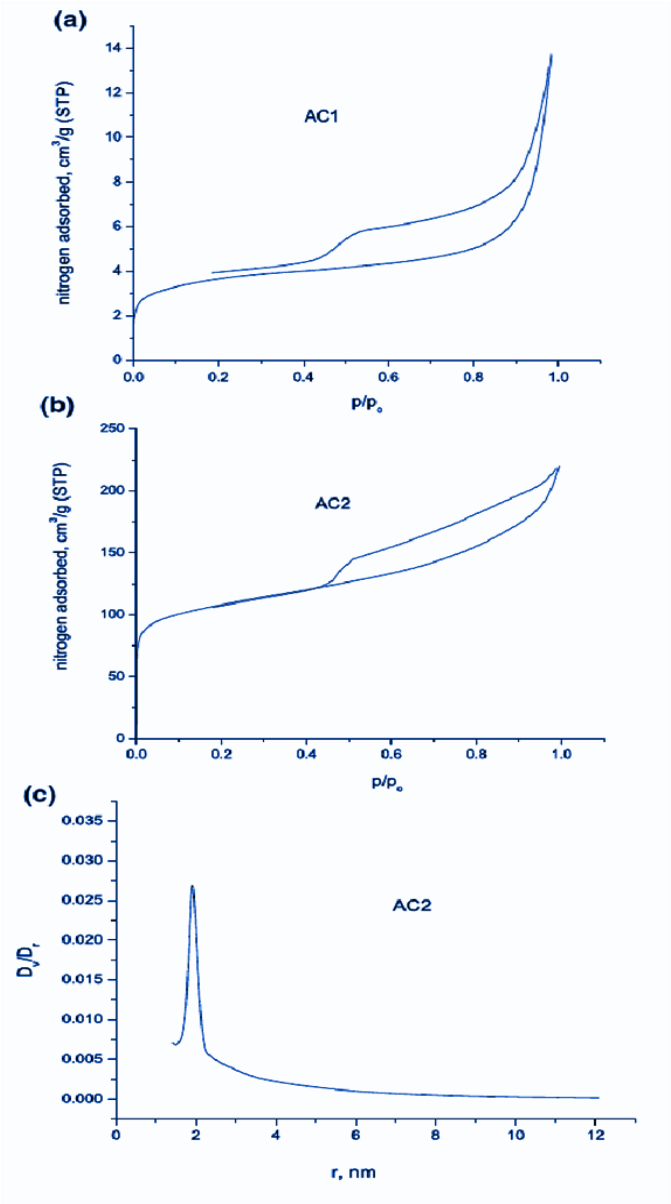

Fig. 21. Adsorption isotherms of the carbonized material AC1 (a) and the activated carbon AC2 (b) derived from algae; pore size distribution of the activated carbon from algae (c)

The adsorption isotherms correspond to a combined type I/IV according to the Brunauer–Deming–Deming–Teller (BDDT) classification, exhibiting a well-defined “knee” at low relative pressures (p/p_0).

Table 15. Textural parameters of the activated carbon derived from algae

Sample	Textural parameters				
	V_{micro} cm^3/g	V_{meso} cm^3/g	V_{micro} %	V_{meso} %	S_{BET} m^2/g
Raw material	0,0052	0,0067	43,7	56,3	13
Activated carbon from algae	0,1512	0,1324	53,3	46,7	501

The data in Table 15 show that steam activation leads to a significant increase in the pore volume and surface area of the resulting activated carbon. It should be noted that the formation of new pores and the development of additional surface area are hindered by the considerable mineral content present in the raw material.

A detailed analysis of the oxygen-containing functional groups on the surface of the activated carbon sample after steam activation is presented in Table 16.

Table 16. Oxygen-containing functional groups on the surface of the activated carbon derived from algae

Sample	**Acidic functional groups**				**Basic functional groups**
	Carboxylic groups	**Lactones**	**Hydroxyl groups**	**Carbonyl groups**	
Activated carbon from algae	0,030	0,110	0,36	1,35	0,842

The Boehm analysis showed that most of the surface functional groups are weakly acidic, although basic groups are also present.

In the precursor – the algae biomass remaining after biodiesel production – a high O/C ratio is observed. This is associated with the high content of oxygen-containing compounds in the raw material.

3.2. Production and characterization of carbon materials (CM) from polystyrene waste and RDF. Application potential

3.2.1. Characterization of CM derived from polystyrene waste

A carbon material was obtained through thermochemical treatment (pyrolysis) of waste polystyrene packaging (Section 2.2.7) and is denoted as (AC X). The pyrolysis of polystyrene (PS) proceeds via a depolymerization mechanism and, at temperatures in the range of 350–

450 °C, leads to a high degree of degradation with the formation of liquid aromatic products– mainly styrene – as well as a solid carbonaceous residue. The elemental composition of the obtained material is presented in Table 17.

Table 17. Elemental analysis of activated carbon AC X

Sample	C %	H %	N %	S %
AB X	79.78	0.46	0.29	0.57

SEM images of sample AB X are presented in Fig. 22.

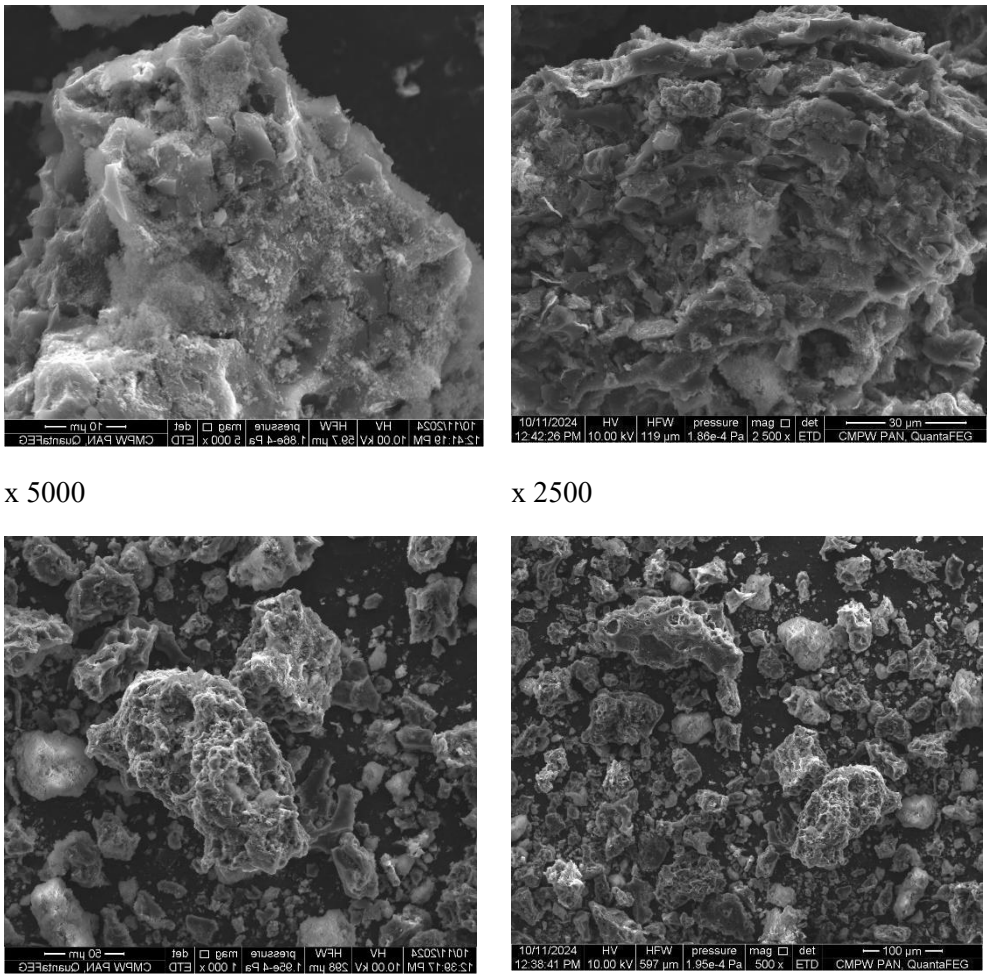

x 5000 x 2500

x 1000 x 500

Fig. 22. SEM images of sample AB X at different magnifications

During the pyrolysis of polystyrene (PS), the material first softens, then foams due to the release of volatile products, leaving behind rough, bubble-like residues that break into irregular, lump-shaped fragments. The SEM images clearly capture this characteristic “foamed” morphology. This behavior is typical for PS-derived chars, as polystyrene lacks an inherent cellular structure, and the volatile products formed during pyrolysis generate random cavities.

At higher magnification, the SEM images reveal a highly fragmented, aggregate-like morphology characteristic of activated carbons produced by pyrolysis followed by activation. Irregular lamellar fragments and torn, plate-like structures are observed, arranged in disordered aggregates. Numerous cavities, crack-like openings, and widened interlayer spaces are visible between them. This morphology corresponds to a hierarchical pore system in which macropores act as transport channels, while mesopores and micropores form between the irregularly stacked graphene-like layers. A "layered," turbostratic appearance is evident.

The nitrogen adsorption–desorption isotherms of the activated carbon sample, measured at 77.4 K, are shown in Fig. 23, and the adsorption–textural parameters calculated from these data are presented in Table 18..

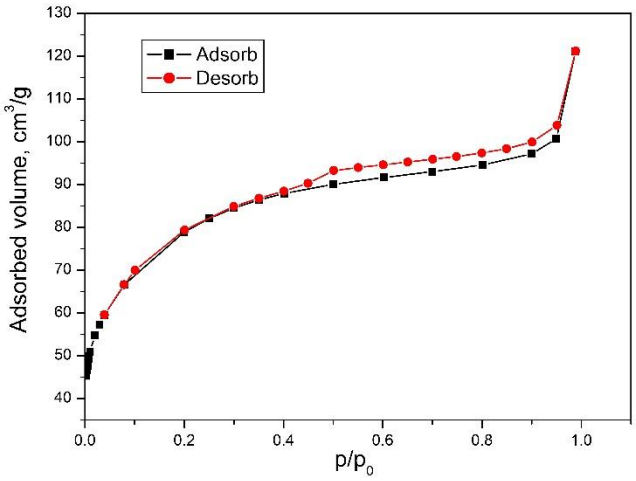

Fig. 23. Low-temperature nitrogen adsorption isotherm (77.4 K) of activated carbon AB X

The nitrogen adsorption–desorption isotherm at 77 K exhibits a well-defined type IV profile accompanied by an H4-type hysteresis loop. This type of hysteresis is characteristic of materials containing a combination of micropores and slit-like mesopores, commonly observed in activated carbons with graphite-like morphology. The steep increase in adsorption at low relative pressures ($P/P_0 < 0.1$) indicates the presence of well-developed microporosity, while the horizontal region and the hysteresis loop in the intermediate range (0.4–0.9 P/P_0) are indicative of a mesoporous structure, likely with a slit-shaped geometry.

Table 18. Specific surface area and main textural parameters of activated carbon AB X

Sample	S_{BET}, m^2g^{-1}	V_{micro}, cm^3g^{-1}	V_{mezo}, cm^3g^{-1}	V_{macro}, cm^3g^{-1}	V_{total}, cm^3g^{-1} *	$V_{0.98}$, cm^3g^{-1}
AB X	1382	0.424	0.284	0.317	1.0250	0.641

The data in Table 18 indicate a well-developed and hierarchically organized pore structure in sample AB X, with a clearly expressed contribution from micro-, meso- and macropores.

First, the high specific surface area (S_{BET} = 1382 m^2/g) is indicative of extensive porosity and a substantial amount of micropores. This is further supported by the micropore volume (V_{micro} = 0.424 cm^3/g), which represents a significant fraction of the total pore volume (V_{total} = 1.025 cm^3/g), i.e., approximately 41%. Such a structure suggests a high adsorption capacity, particularly toward small molecules.

The mesopore volume (V_{meso} = 0.284 cm^3/g, ~28%) is also considerable, which is important for facilitating the diffusion of adsorbates toward the active sites located within the micropores. The presence of macropores (V_{macro} = 0.317 cm^3/g, ~31%) further enhances mass transport throughout the material.

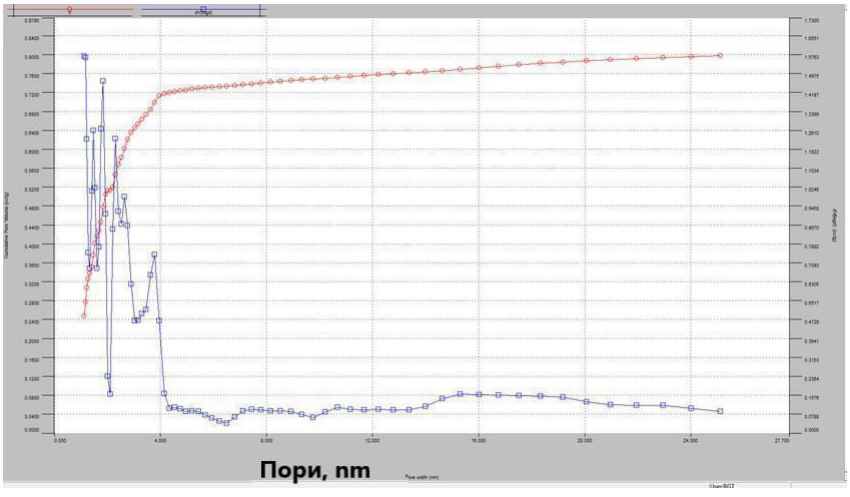

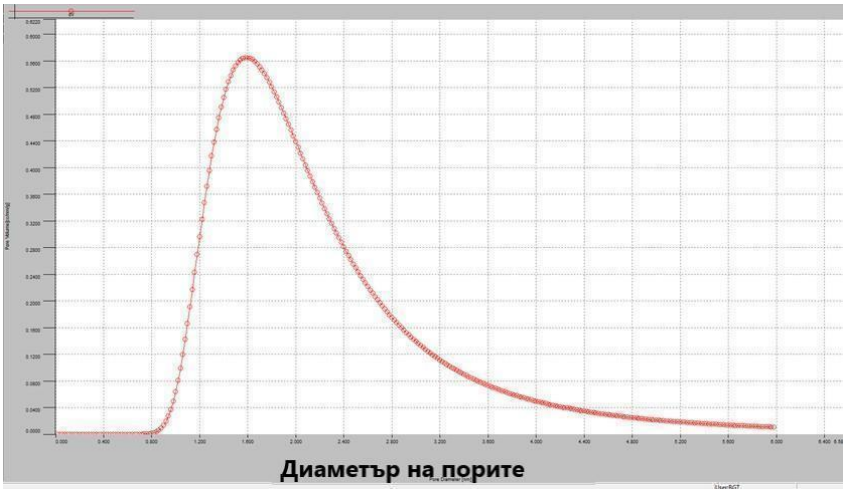

Fig. 24. Pore size distribution (nanometers

Sample AB X is characterized by a hierarchical micro–meso–macroporous structure, combining high adsorption capacity (due to the micropores) with good transport properties (due to the meso- and macropores). The FTIR spectrum of the carbon material is presented in Fig. 25.

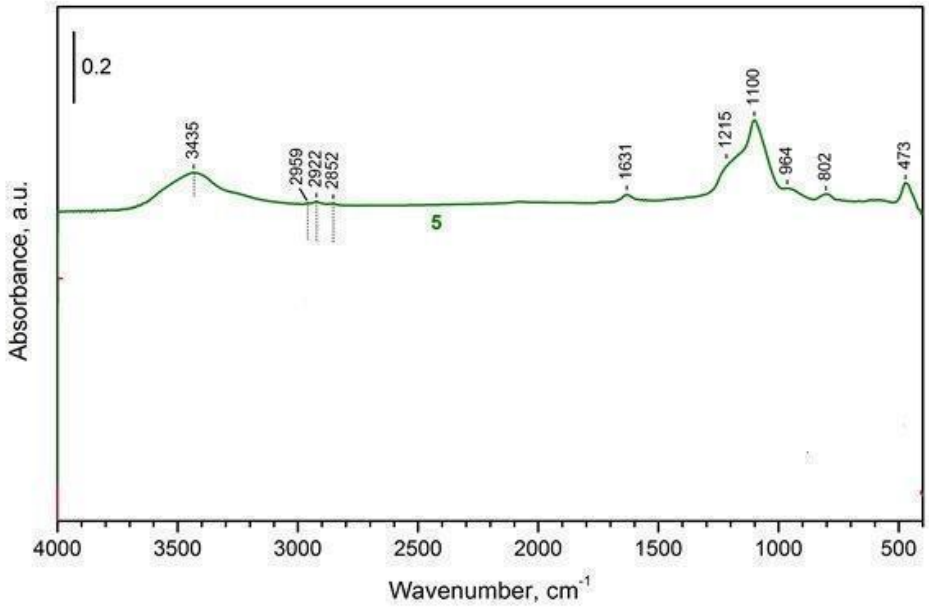

Fig. 25. FTIR spectrum of the adsorbent AB X

In the spectrum, the bands corresponding to specific surface functional groups cannot be identified unambiguously, but it can be noted that the broad peak at 3435 cm^{-1} indicates the presence of hydroxyl groups. The bands around 2950 cm^{-1} are attributed to aliphatic C–H structures. The peaks near 1630 cm^{-1} may be associated with C=O stretching vibrations. The peak at 1215 cm^{-1} corresponds to C–O bonds from ester groups or lactones, while the band at 1100 cm^{-1} is assigned to S=O vibrations, likely originating from the sulfuric acid treatment.

From the analysis of the FTIR spectrum, it can be concluded that oxidation of the precursor with H_2SO_4 expectedly leads to the formation of oxygen-containing functional groups.

The structure of the carbon material was also examined by Raman spectroscopy (Fig. 26).

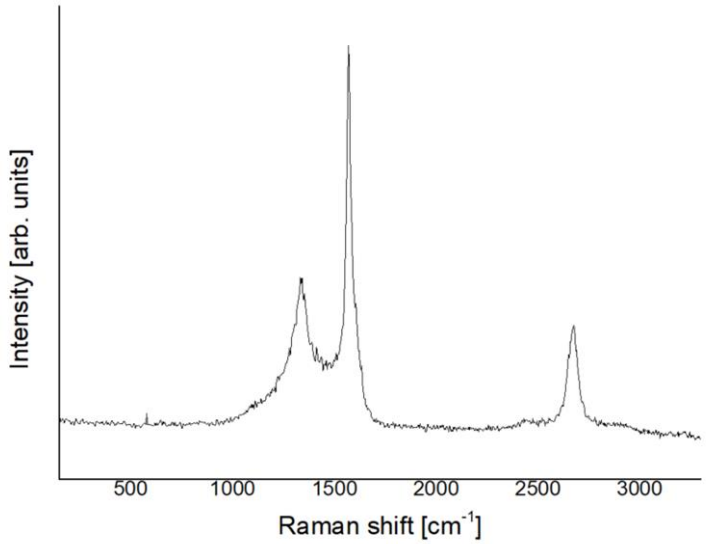

Fig. 26. Raman spectrum of sample AB X

The Raman spectrum of the investigated carbon material (X) is characterized by two well-defined bands – the D-band at approximately 1350 cm^{-1} and the G-band at ~1580–1600 cm^{-1}–as well as a weaker, broad band in the region around 2700 cm^{-1} (the 2D-band). The intensity ratio ID/IG is relatively high, indicating a significant degree of structural disorder and the presence of small graphite-like domains. This is typical of a turbostratic structure, in which the graphene layers are misaligned and poorly ordered in three-dimensional space.

The results obtained from the Raman analysis correlate well with the adsorption–textural data, which show a high specific surface area and a well-developed porous structure. The Raman spectrum confirms that the studied material is a highly defective, turbostratic carbon with a low degree of crystallinity and a well-developed network of sp^2-hybridized domains–features that are conducive to high adsorption activity and suggest potential applicability in adsorption and catalytic processes

3.2.2. Application of AB X for the removal of the textile dye Drimaren Red (DrR) from aqueous solutions

The obtained activated carbon AB X possesses a high specific surface area, which suggests its effectiveness in the adsorption of organic compounds from aqueous solutions. The change in dye concentration in the solutions was monitored using a UV–Vis spectrophotometer, with absorbance measured at a wavelength of $\lambda = 548$ nm. The amount of adsorbed dye (adsorption capacity) was calculated according to equation (1) in Section 3.1.4.

During the adsorption experiments, the time required to reach adsorption equilibrium was determined at the highest pollutant concentration used (100 mg L^{-1}). For this purpose, a kinetic analysis was performed, in which the change in sorption capacity over time was monitored.

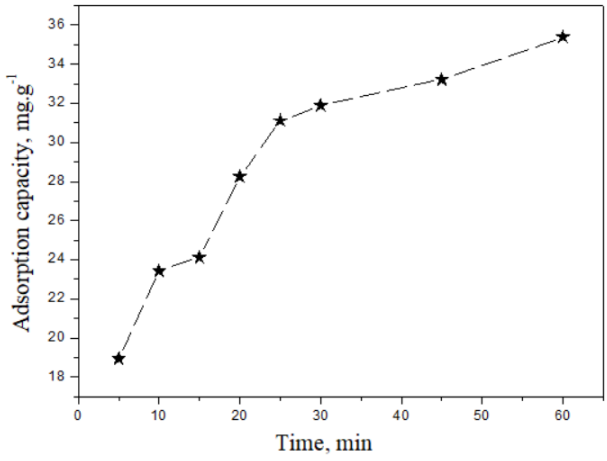

Fig. 27. Adsorption kinetics of DrR from aqueous solution using the adsorbent AB X

The change in adsorption capacity over time shows a rapid increase during the first 20–30 min, followed by a gradual leveling-off of the curve (Fig. 27).

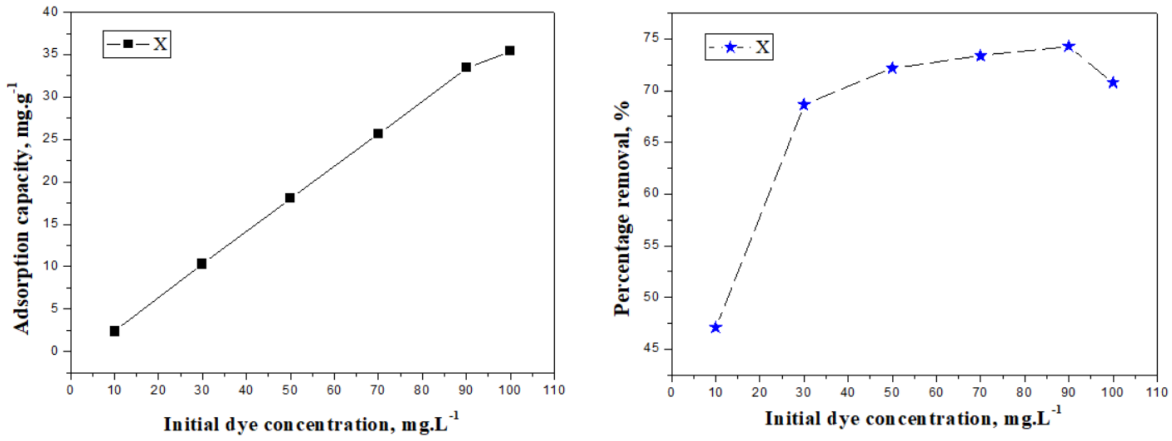

Fig. 28. Effect of dye concentration on adsorption capacity and removal efficiency

The experimental data (Fig. 28) show that with increasing initial dye concentration, the adsorption capacity of the adsorbent increases almost linearly, which indicates the presence of available active sites and efficient retention of dye molecules at higher concentrations.

In addition to the effect of initial concentration on the adsorption process, the influence of temperature on the adsorption kinetics was also investigated.

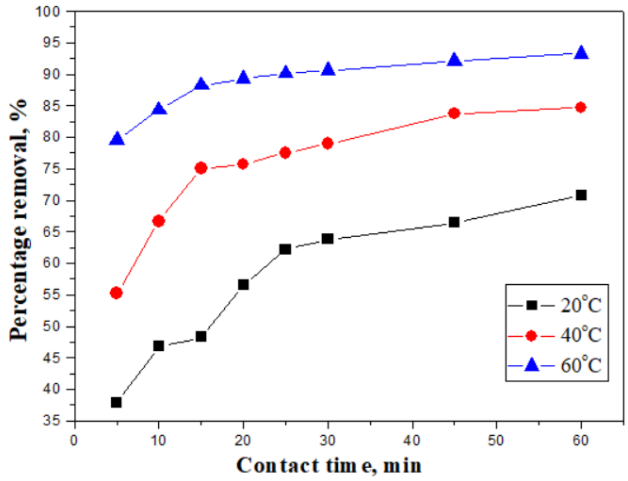

Fig. 29. Effect of temperature on the amount of adsorbed reactive dye

The experimental data (Fig. 29) show that with increasing contact time, the percentage of adsorbed dye increases until nearly constant values are reached, indicating the establishment of adsorption equilibrium. A clear temperature effect is observed—the highest adsorption percentage is recorded at 60 °C. This behavior demonstrates that increasing the temperature accelerates the adsorption process and enhances dye uptake, which is indicative of an endothermic adsorption mechanism.

The adsorption capacity of the investigated carbon material increases with rising initial concentration of Drimaren Red in the aqueous solution and reaches a value of 35 mg/g, confirming the good potential of the material for water purification applications.

Kinetic modeling shows that the process is best described by the pseudo-second-order equation, suggesting a chemisorption mechanism involving electron exchange or the formation of chemical bonds between adsorbate and adsorbent.

The material derived from waste plastic exhibits the highest degree of graphitization and the best electrical conductivity, which implies strong potential for applications in catalytic and electrochemical systems—an aspect that remains to be further investigated.

3.2.3. Characterization of RDF-based adsorbents

Nitrogen physisorption of the RDF-derived adsorbent

The adsorbent obtained from RDF was analyzed by low-temperature nitrogen adsorption. The data in Table 19 and Fig. 30 show that, in terms of textural parameters, satisfactory results were achieved for the carbon adsorbents produced by pyrolysis, including pore texture and pore size distribution. All samples are characterized by a moderate specific surface area (300–750 m^2/g) and the presence of both micro- and mesopores. Due to the specific nature of the

synthesis of carbon foam, it was necessary to apply steam activation (hydropyrolysis) to generate micro- and mesopores and to obtain a higher surface area.

Table 19. Textural parameters of the adsorbents used

Sample	S_{BET} m^2/g	V_{micro} cm^3/g	V_{meso} cm^3/g	ЙЧ mgJ/g
Adsorbent A	374	0,148	0,030	430
Adsorbent B	320	0,128	0,005	390
Adsorbent C	285	0,108	0,006	345
Adsorbent D	768	0,260	0,003	850

The pore size distribution of the VM samples obtained from RDF, determined by the DFT method, is presented in Fig. 30.

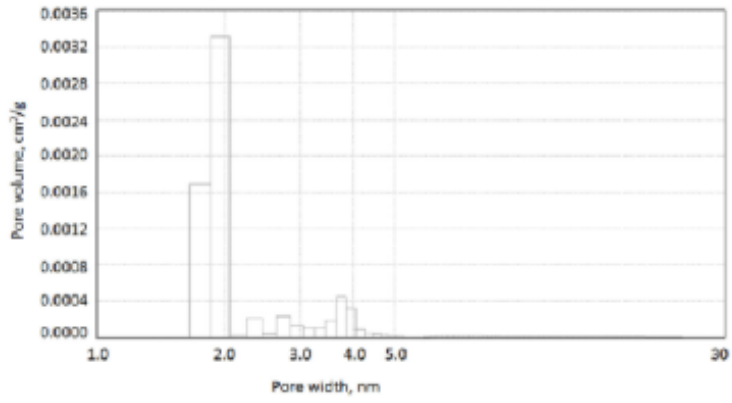

Sample A

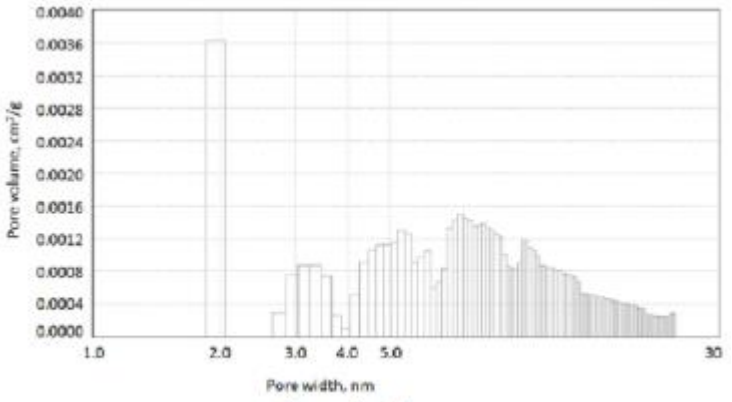

Sample B

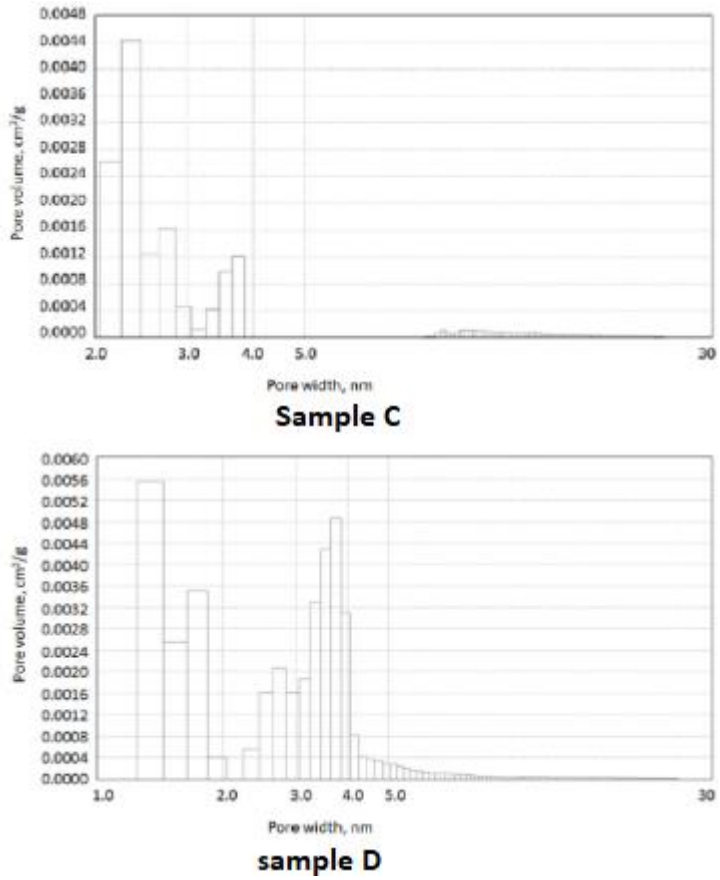

Fig. 30. Pore size distribution (DFT method) of the AB samples derived from RDF

The pore size distribution of the four carbon materials shows clearly distinguishable differences in their structural characteristics. Sample **A** exhibits the narrowest and most uniform distribution, with the pore volume concentrated almost entirely around 2–2.3 nm and minimal presence of wider pores. This indicates a monomodal structure with a high degree of uniformity.

Sample **B** displays a significantly broader and more complex distribution, containing both narrow pores around 2 nm and a substantial amount of mesopores in the 3–6 nm range, along with an extended tail reaching up to approximately 30 nm. Such a profile is characteristic of a well-developed hierarchical pore structure (a multilevel, interconnected porosity spanning nano-, meso-, and macro-scale domains).

Sample **C** combines a primary maximum in the 2–2.5 nm region with a secondary group of pores between 3 and 4.5 nm, without notable extension toward larger pore sizes. Thus, its structure is bimodal but less hierarchical compared to sample B.

Sample **D** exhibits the most developed and voluminous pore network, consisting of several clearly distinguishable pore groups—narrow pores in the 1.5–2.5 nm range, a well-defined second maximum around 3–4 nm, and a weak but extended tail toward larger pore sizes. This sample also possesses the highest total pore volume.

3.2.4. Characterization of activated carbon obtained from bituminous waterproofing material (BWM)

The results are presented in Table 20.

Table 20. Elemental analysis of activated carbon derived from BWM

Sample	C, wt. %	C, mol	H, wt. %	H, mol	N, wt. %	N, mol	S, wt. %	S, mol
RDF (BW)	47.1	3,925	2.25	2.25	4.2	0.3	2.3	0.07

The textural properties of the adsorbents were investigated by nitrogen adsorption–desorption at −196 °C. Prior to the measurements, the samples were heated at 300 °C for 4 h to remove volatile components and moisture.

Table 21. Specific surface area and pore volume of activated carbon derived from BWM

Sample	S_{BET} m^2g^{-1}	V_{total}, cm^3g^{-1}	V_{micro}, cm^3g^{-1}	V_{mezo}, cm^3g^{-1}	V_{macro}, cm^3g^{-1}
RDF	713	0.122	0.097	0.019	0.006

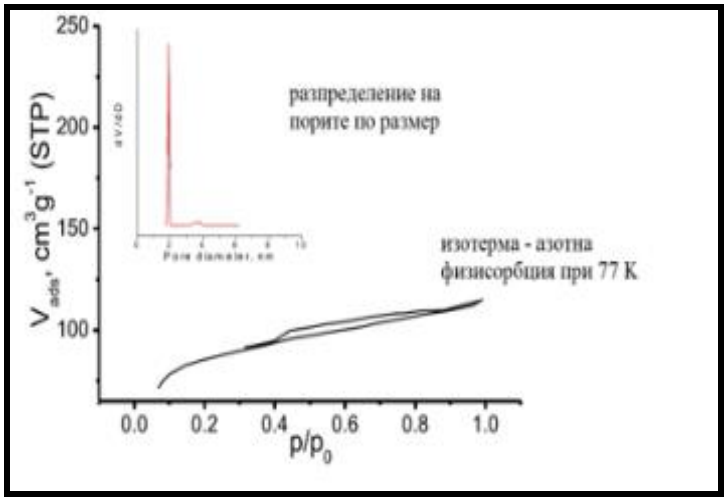

Fig. 31. Adsorption isotherm and pore size distribution

From the data presented in Table 21 and Fig. 31, a predominance of micropores is observed, with a pore volume of 0.097 $cm^3 \cdot g^{-1}$, confirming the nanoporous structure of the adsorbent. The pore volume was calculated using the Dubinin–Radushkevich method, while the macropore volume was determined as the difference between the total pore volume and the sum of the micropore and mesopore volumes. The carbon-to-hydrogen molar ratio, calculated as 3.95 / 2.25 = 1.756, provides information about the degree of carbonization of the material.

Experimental studies were also conducted to evaluate the applicability of the obtained adsorbent for water purification from different dyes, such as methyl orange and bromothymol blue, and the results are presented in Fig. 32.

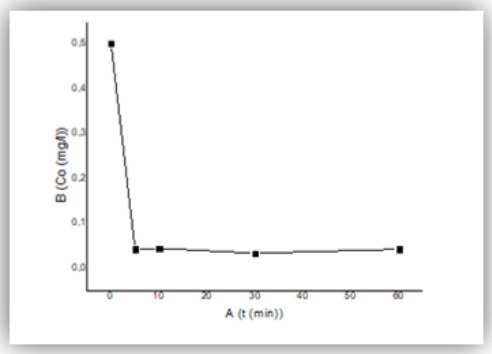
B (Co (mg/l))
A (t (min))

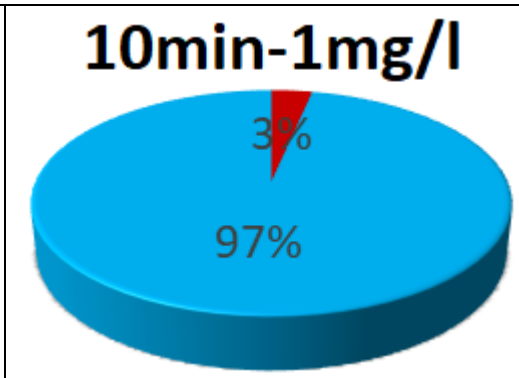
10min-1mg/l
3%
97%

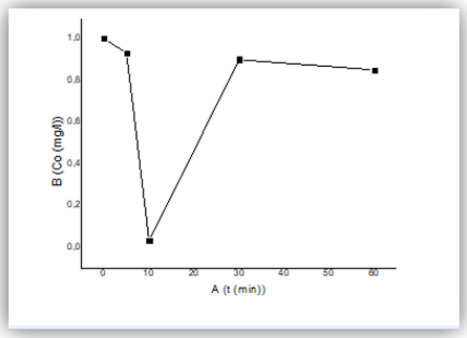
B (Co (mg/l))
A (t (min))

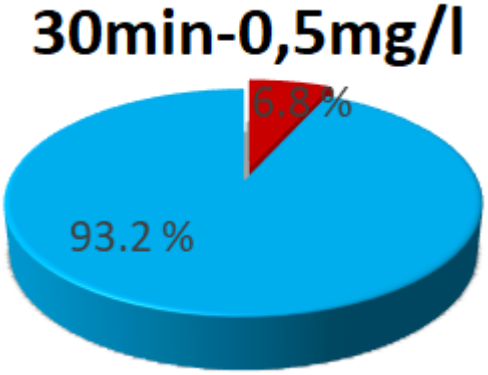
30min-0,5mg/l
6.8 %
93.2 %

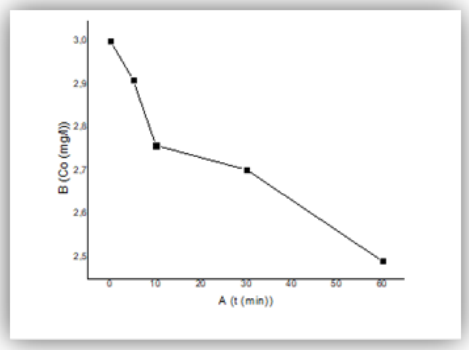
B (Co (mg/l))
A (t (min))

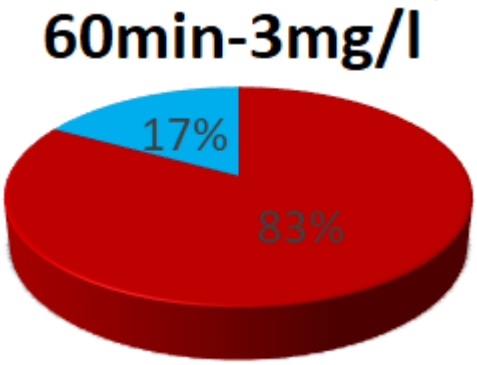
60min-3mg/l
17%
83%

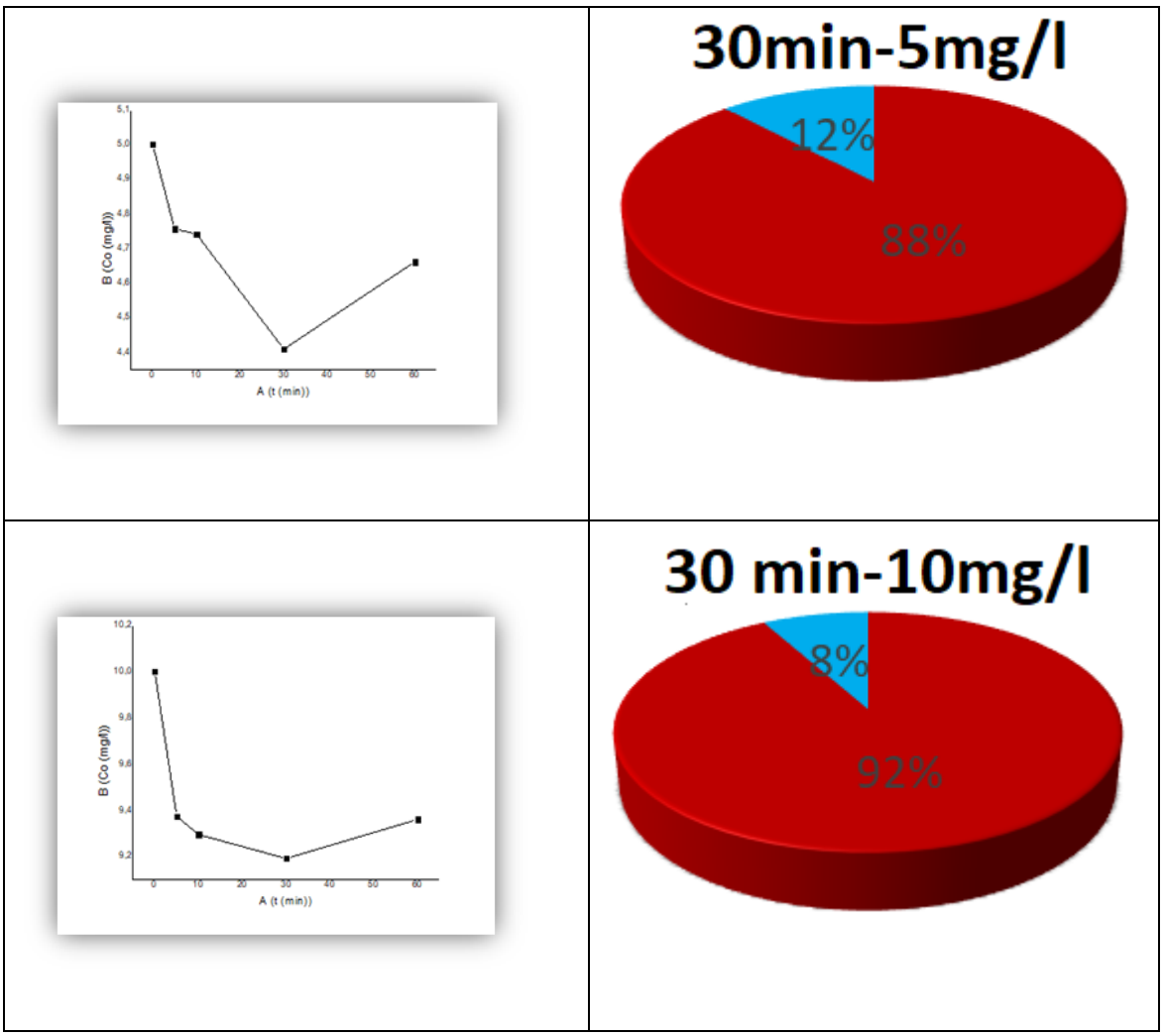

Fig. 32. Adsorption of methyl orange

Methyl orange exhibits typical behavior of an anionic monoazo dye containing sulfonate groups during adsorption onto activated carbon. The obtained experimental data (Fig. 32) show that the activated carbon exhibits a high adsorption capacity toward methyl orange, with the process proceeding rapidly during the first 10–20 minutes, followed by a gradual stabilization and the establishment of adsorption equilibrium.

At low initial concentrations (0.5–1 mg·L^{-1}), the adsorption efficiency is maximal (above 93–97%), indicating the presence of a large number of available active sites and effective dye uptake. The observed decrease in adsorption efficiency with increasing concentration is characteristic of systems well described by the Langmuir isotherm.

The results confirm that the retention mechanism is predominantly physical adsorption with fast kinetics governed by external diffusion, followed by equilibrium establishment. The observed behavior is typical for anionic azo dyes adsorbed onto activated carbon.

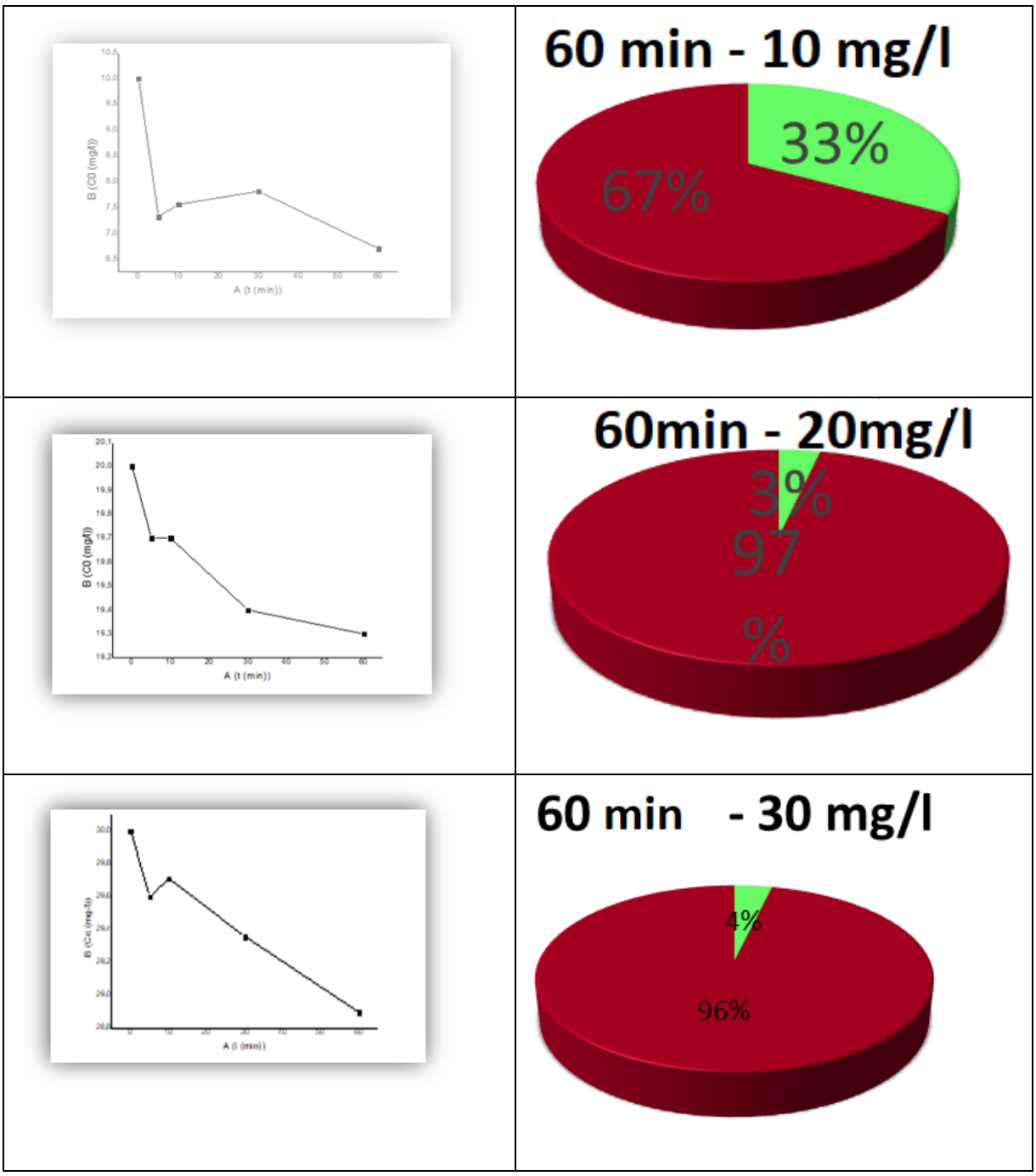

Fig. 33. Adsorption of Bromothymol Blue (BTB)

The results presented in Fig. 33 show that with increasing initial dye concentration, the efficiency of the process decreases significantly. At 10 mg·L⁻¹, adsorption is limited but still noticeable (approximately 30%). At 20 mg·L⁻¹, it decreases to only 9%, and at 30 mg·L⁻¹ it reaches minimal values of 4%, indicating near-complete saturation of the adsorbent.

This behavior is characteristic of sulfonephthalein dyes with larger molecular structures, such as Bromothymol Blue. Due to its considerable size and steric bulk, the molecule has limited access to the micropores of activated carbon and occupies only a small fraction of the

mesopores. The results indicate that the adsorption behavior of BTB is significantly more restricted compared to methyl orange and is mainly governed by kinetic and structural limitations related to dye diffusion within the carbon pore system.

3.2.5. Synthesis and characterization of carbon foam based on coal tar and furfural

The obtained carbon foam samples were characterized by XRD, scanning electron microscopy (SEM), TEM and EDS, TG, DSC analyses, and elemental analysis. The proposed new, less energy-intensive synthesis method enables the production of carbon foam with very good physicochemical properties.

Elemental analysis

Table 22. Elemental analysis of carbon foam samples synthesized by HNO_3 and H_2SO_4 treatment from mixtures containing 50% coal tar and 50% furfural

Sample	C	H	N	S	O	C/H
	wt%					
CFFS50	89.32	1.81	0.63	1.42	6.82	4.11
CFFN50	84.31	1.94	2.72	0.57	10.46	3.62

Thermal analysis of the carbon foam samples was performed using thermogravimetric analysis (TG) and differential scanning calorimetry (DSC). The results are presented in Fig. 34.

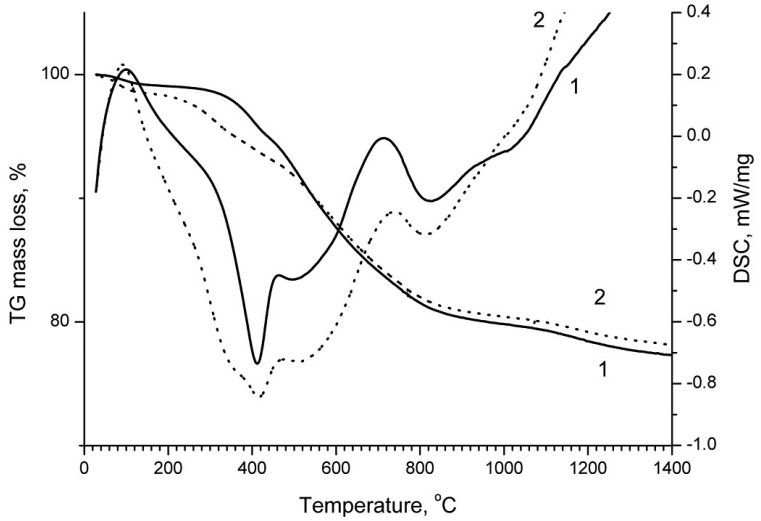

Fig. 34. TG and DSC analysis (exothermic effects downward) of carbon foam samples synthesized by HNO_3 (1) and H_2SO_4 (2) treatment from mixtures containing 50% coal tar and 50% furfural

X-ray diffraction analysis of carbon foam

The obtained results show that the structure of the produced carbon foam strongly depends on the chemical composition of the precursor and the synthesis method.

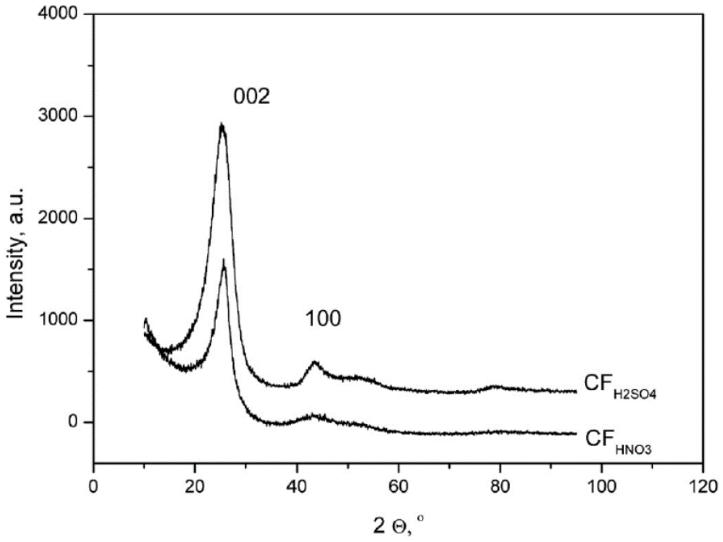

Fig. 35. X-ray diffraction analysis of the obtained carbon foam

In the X-ray diffraction pattern of CFFS, a strongly intense and narrow (002) peak is detected, corresponding to the interplanar spacing in the carbon lattice. This is a clear indication of a relatively high degree of graphitization and the presence of a well-ordered structure, in contrast to the sample obtained from pitch modified with nitric acid. After activation of the carbon foam samples, a more disordered structure is observed in all cases, which is reflected in a slight broadening of the (002) peak (at 2θ = 24°) and the (100) peak (at 2θ = 44°) in the X-ray diffraction patterns.

Scanning electron microscopy (SEM) of carbon foam

For morphological characterization of the samples by SEM, an FEI Quanta 250 FEG electron microscope was used.

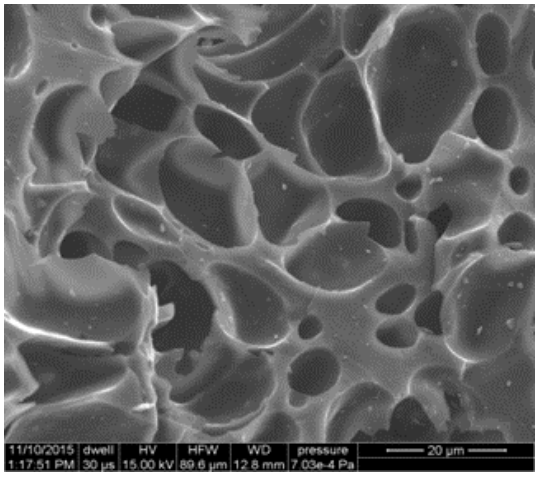

1

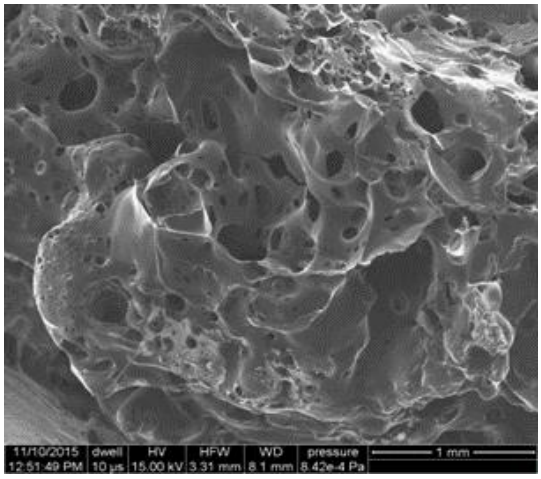

2

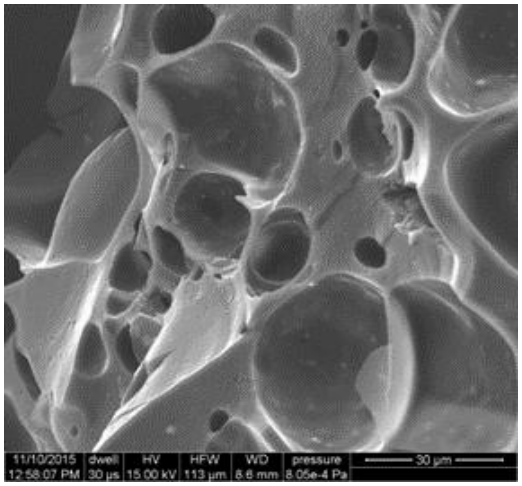

3

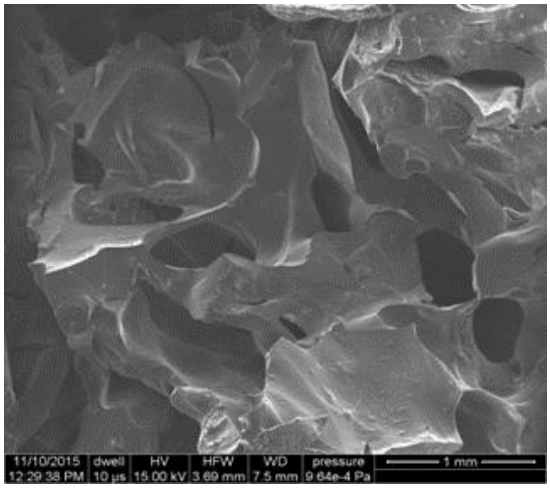

4

Fig. 36. Scanning electron microscopy images of carbon foam samples obtained from a coal tar pitch and furfural mixture (1:1.5), modified with HNO_3 (1 and 2) and H_2SO_4 (3 and 4)

A **B**

Fig. 37. Photographic images of carbon foam samples. (A) after treatment with H_2SO_4 and (B) after treatment with HNO_3

The SEM results show that the carbon foam obtained from pitch modified with HNO_3 is characterized by relatively uniform macropores with sizes of 200–250 μm, whereas the carbon foam derived from pitch modified with H_2SO_4 exhibits open macropores with sizes of 300–350 μm. The electron microscopy images clearly reveal microcracks, which are characteristic of high-quality carbon foam. These microcracks are mainly formed between the graphitic layers parallel to the macropore walls, particularly in the space between the macropores. No large cracks are observed on the macropore walls of the obtained carbon foam samples.

3.3. Preparation of catalysts based on activated carbon from almond shells

3.3.1. Characterization of activated carbon and catalysts

Elemental analysis of almond shells showed that they contain approximately 50% C, 5.3% H_2, 0.8% N_2, and a minimal amount of sulfur. The proximate analysis of the sample indicates a high content of volatile matter (73%) and a low ash content.

Table 23. Elemental and proximate analysis of the precursor, activated carbon, and ACZn and AC18 catalysts.

Sample	Elemental analysis				Technical analysis	
	C, %wt	H, %wt	N, %wt	S, %wt	Vol. Mat, %wt	Ash, %wt
Almond shell	49.59	5.32	0.8	0.1	72.91	1.36
AC	84.6	1.82	0.65	0.05	10.40	3.93
AC18M	82.06	1.42	0.60	2.52	10.23	3.32
ACZn	78.19	1.70	0.30	0.04	11.54	5.44

The morphology of activated carbon (AC) and the catalysts (ACZn and AC18) was examined using scanning electron microscopy (SEM). Fig. 38 shows the surface morphology of the activated carbon obtained from almond shells and the functionalized samples after treatment with Zn and sulfuric acid (18 M). As a result of the hydrothermal pyrolysis treatment of almond shells, the obtained activated carbon is characterized by a surface with pores of various shapes and sizes. After chemical activation and modification of the sample with $ZnCl_2$, Zn particles are mainly deposited on the carbon surface, giving the sample a rough texture.

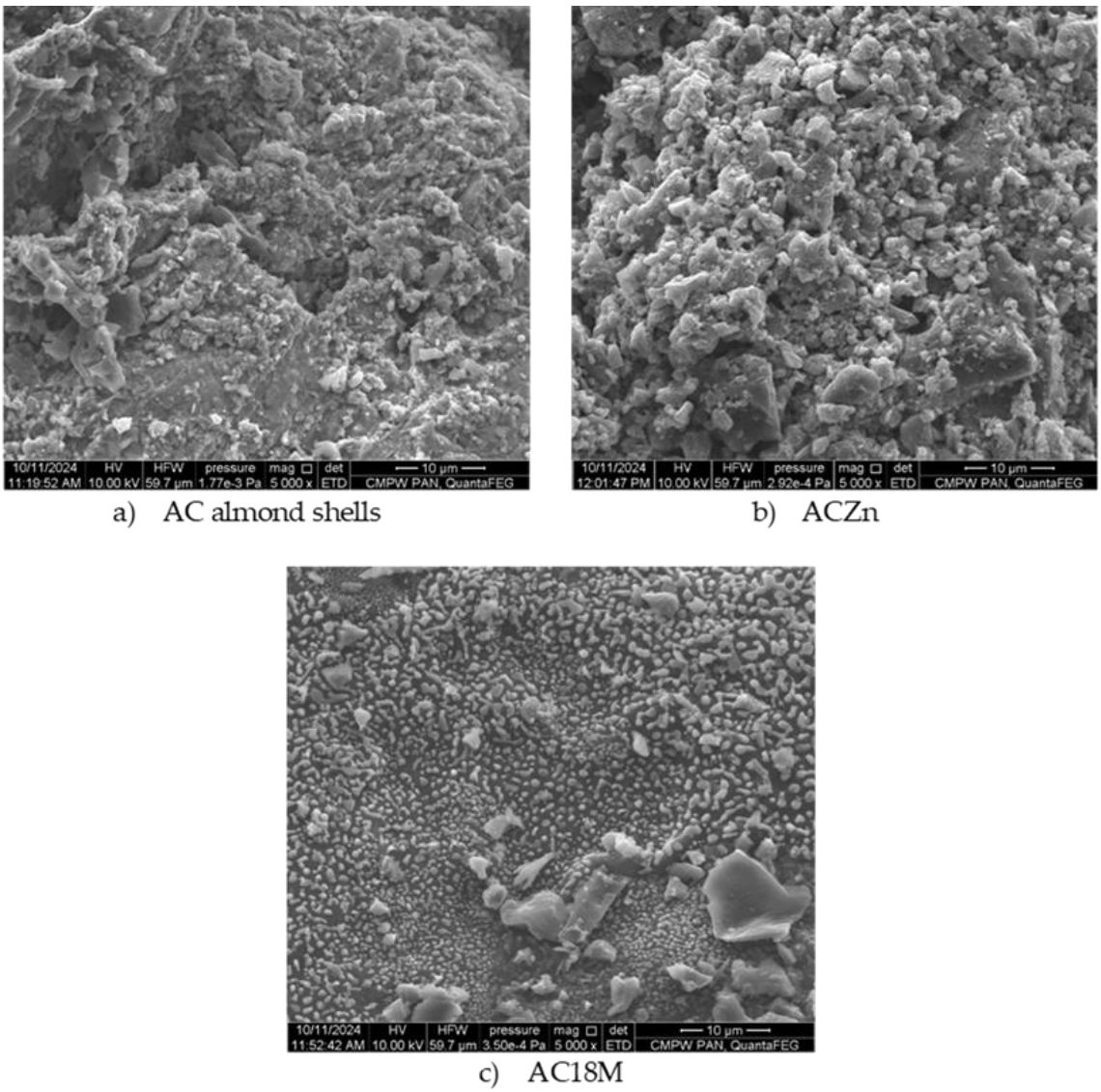

Fig. 38. SEM images of activated carbon from almond shells: A) AC, B) ACZn, C) AC18M

During the functionalization of activated carbon with sulfuric acid, the interaction between the acid and surface carbon atoms leads to smoothing of the surface edges. These results are consistent with the textural characteristics observed for the samples, as presented in Table 23 and Fig. 38.

Energy-dispersive X-ray analysis (EDX) was used to determine the elemental composition of the $ZnCl_2$-modified activated carbon, with particular emphasis on the zinc content. The results show that the content of metallic particles is 4.47%, indicating that during the impregnation/activation step only about 50% remained on the catalyst.

The specific surface area calculated according to the Brunauer–Emmett–Teller (BET) theory, the total pore volume, pore diameter, and pore size distribution were determined using Quenched Solid Density Functional Theory (QSDFT) based on N_2 physisorption analysis (Table 24, Fig. 39). The results show that the surface area and total pore volume of ACZn are higher

(604 $m^2 \cdot g^{-1}$ and 0.30 $cm^3 \cdot g^{-1}$, respectively), most likely due to activation during treatment with zinc chloride, compared to AC (452 $m^2 \cdot g^{-1}$ and 0.22 $cm^3 \cdot g^{-1}$). In catalytic reactions, the high specific surface area of microporous materials provides a large number of active sites for interaction with reactants [125]. The ACZn catalyst exhibits a micro–mesoporous structure, where small channels and cavities increase the specific surface area and facilitate access of reactant molecules (glucose molecules with a size of 0.9–1 nm) to the active metal sites. Mesopores, in turn, improve the transport of reactants and products by reducing diffusion limitations.

The specific surface area of the material obtained after sulfonation of the initial AC sample decreases slightly (from 452 to 441 $m^2 \cdot g^{-1}$), likely due to partial destruction of mesopores on the AC surface. However, the purpose of sulfonation is the formation of Brønsted acid active sites on the material surface.

Table 24. Textural properties of activated carbon (AC) and catalysts ACZn and AC18M

Textural properties	AC	ACZn	AC18M
Specific surface area (S_BET, $m^2 \cdot g^{-1}$)	452	604	441
Total pore volume (V_{tot}, $cm^3 \cdot g^{-1}$)	0.22	0.30	0.22
Micropore volume ($V_{mi}c$, $cm^3 \cdot g^{-1}$)	0.149	0.197	0.144
Mesopore volume (V_{mes}, $cm^3 \cdot g^{-1}$)	0.072	0.106	0.068
Pore diameter (QSDFT, nm)	1.01	0.67	1.01

The micropore volume in the three samples, relative to the total pore volume, varies within a narrow range (65–67%).

The catalyst activated with $ZnCl_2$ shows approximately a 44% decrease in the average pore diameter compared to the initial activated carbon (AC) and the modified sample (AC18M), most likely due to the penetration of zinc particles into the pores during the impregnation step. The pore size distributions obtained by QSDFT are presented in Fig. 37.

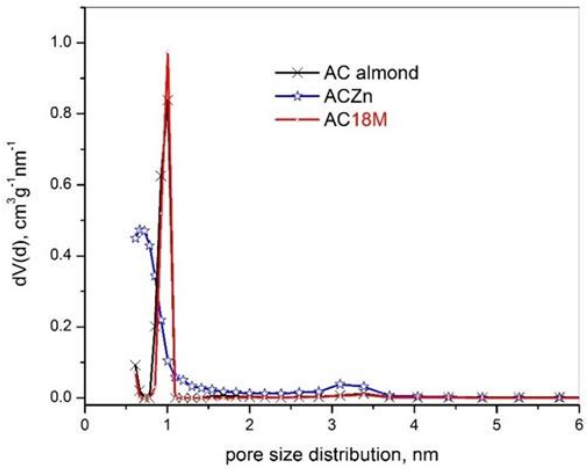

Fig. 39. Pore size distribution of the initial activated carbon and the AC18M and ACZn catalysts

The zinc-modified catalyst is characterized predominantly by micropores smaller than 0.8 nm and mesopores with an approximate size of 3 nm.

The textural characteristics of activated carbon (AC) and the synthesized samples ACZn and AC18M were determined by nitrogen adsorption isotherm analysis. The obtained nitrogen adsorption–desorption isotherms are presented in Fig. 40.

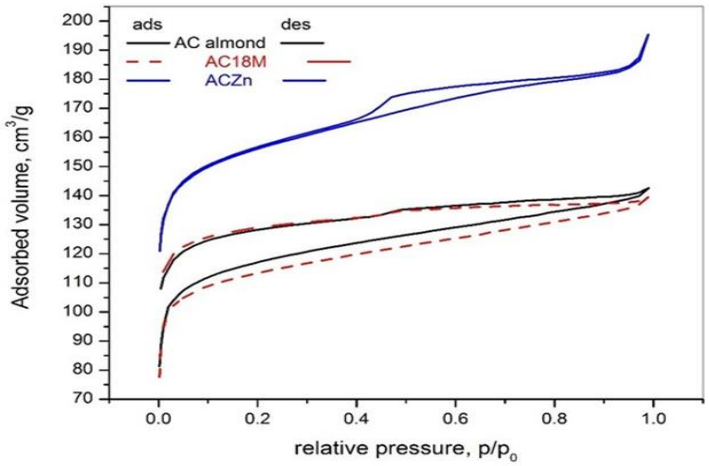

Fig. 40. N_2 physisorption analysis of activated carbon (AC) and catalysts ACZn and AC18M

The surface chemistry of the obtained catalysts was characterized by X-ray photoelectron spectroscopy (XPS). The binding energies (BE) of activated carbons measured by this method depend on their chemical structure and the type of functional groups present on the surface.

The results of the XPS analysis confirmed the presence of SO_3H groups as a result of surface functionalization of AC with sulfuric acid. The XPS spectra (Fig. 41) show well-defined

components of sulfur-containing species on the material surface. Sulfoxide groups are observed at a binding energy of 164.2 eV, while sulfonic acid functional groups are identified at 168.5 eV.

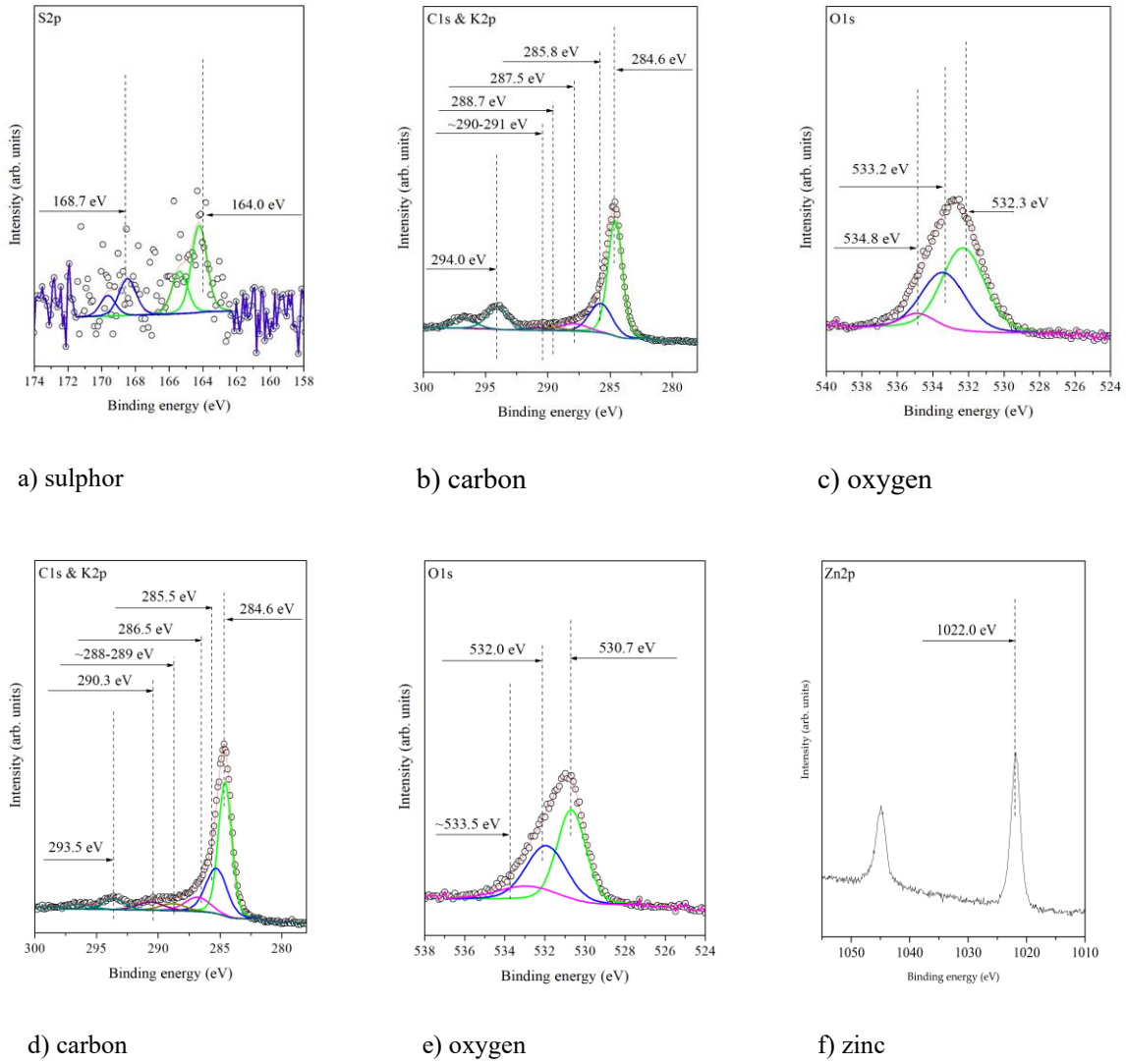

a) sulphor b) carbon c) oxygen

d) carbon e) oxygen f) zinc

Fig. 41. XPS spectra of catalyst AC18M (a–c) and ACZn (d–e)

The results from the C1s XPS spectra of the two samples (Table 25) show main peaks with binding energies corresponding to sp^2 and sp^3 carbon, as well as oxygen-containing functional groups, namely C–O, C=O, and O–C=O. For the ACZn catalyst, the total carbon content is 68.7% (surface atomic concentrations, %at.). The results confirm that chemical functionalization with both $ZnCl_2$ and sulfonation leads to an increased oxygen content in the carbon material.

As expected, zinc is detected in the Zn-impregnated catalyst (6.8%). The ACZn spectra show the characteristic Zn 2p doublet at 1045 and 1021.9 eV (Fig. 41e), corresponding to Zn in a

ZnO lattice with a wurtzite structure. The oxygen signal associated with the ZnO lattice is observed at 530.5 eV.

Table 25. Results of X-ray photoelectron spectroscopy (XPS) analysis.

Sample		ACZn	AC18M
S 2p	BE, eV	% At конц.	% At конц.
$S(=O)_2$	164.2	n.d.	0.3
$-SO_3H$	168.5	n.d.	0.1
C 1s			
C-C (sp^3)	284.6	35	46.3
C-O	285.5	18.9	18.3
C=O	287	6.9	5.4
O-C=O	289	3.5	2.9
π-π	291	4.2	1.6
Total C %At Conc	C 1s	**68.7**	**74.4**
O 1s			
Zn=O	530.9	8.6	n.d.
O-C=O	532	7.1	7.8
anhydrides or lactones	532.9	2.6	n.d.
S=O	533.4	n.d.	5.5

H_2O (ads.)	534.9	n.d.	1.1
Total O %At Conc		**18.3**	**14.3**
Zn $2p_{3/2}$	1021.9	6.8	0.6

The powder X-ray diffraction (PXRD) analysis (Fig. 42) of the activated carbon sample shows the formation of activated carbon from almond shells, as indicated by two broad diffraction peaks at 2θ = 24° and 43°.

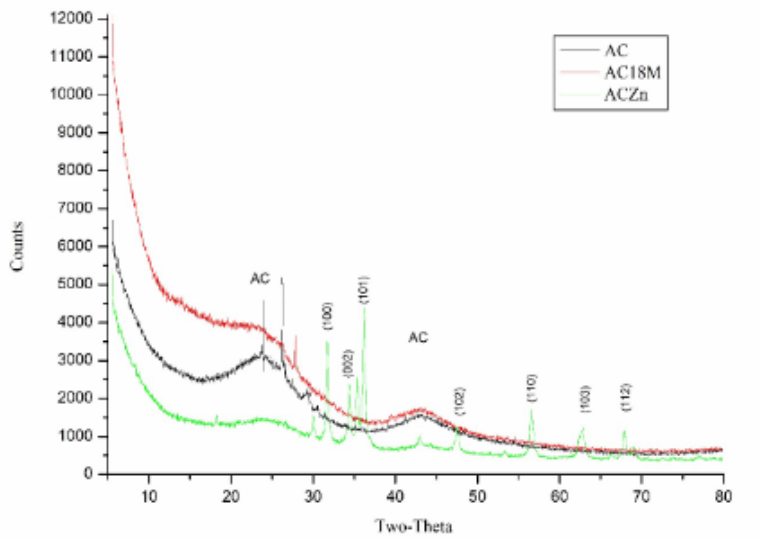

Fig. 42. Powder X-ray diffraction (PXRD) patterns of activated carbon (AC), AC18M, and ACZn

These peaks are characteristic of the amorphous structure of activated carbon. The diffractogram also shows several typical diffraction peaks of ZnO in the 2θ range of 30–70°, which are consistent with the hexagonal wurtzite structure of ZnO (JCPDS No. 79-2205). The peaks are observed at 2θ = 31.6°, 34.5°, 35.4°, 36.2°, 47.0°, 56.2°, 62.8°, and 68.1°. No peaks corresponding to $ZnCl_2$ or metallic Zn are detected.

The FTIR spectra of activated carbon and catalysts are shown in Fig. 43. The broad band at around 3435 cm^{-1} in the FTIR spectra of all samples is characteristic of hydroxyl group presence. Absorption bands in the range of 2950 cm^{-1} and 2850 cm^{-1} correspond to C–H stretching vibrations associated with aliphatic (C–H) groups.

In the spectra of AC and AC18M samples, peaks around 1741 cm^{-1} are observed (associated with carboxylic groups, anhydrides, and lactones), indicating the presence of carbonyl (C=O) functionalities. Bands around 1630 cm^{-1} may be attributed to aromatic ring vibrations associated with C=O, C=C bonds, or OH groups. The peak around 1570 cm^{-1} is likely

related to C=C stretching vibrations of aromatic rings, and these bands are observed in all samples (AC, AC18M, and ACZn). In the AC spectrum, an absorption band is detected at 1430 cm^{-1}, attributed to deformation bending of methylene groups.

Bands appearing in the region 1292–1269 cm^{-1} can be assigned to C–O stretching vibrations in acidic, phenolic, or ether structures (symmetric vibrations). The bands at 1152 cm^{-1} ($–SO_3H$) and 1105 cm^{-1} (symmetric vibrations of O=S=O) in the spectrum indicate that sulfonic acid groups are successfully incorporated onto the catalyst surface [134]. Absorptions due to γ(C–H) vibrations appear at around 876 cm^{-1} (AC and AC18M).

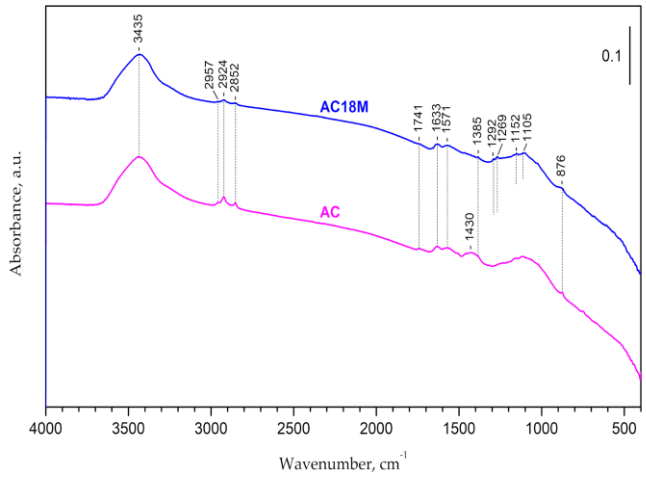

(a)

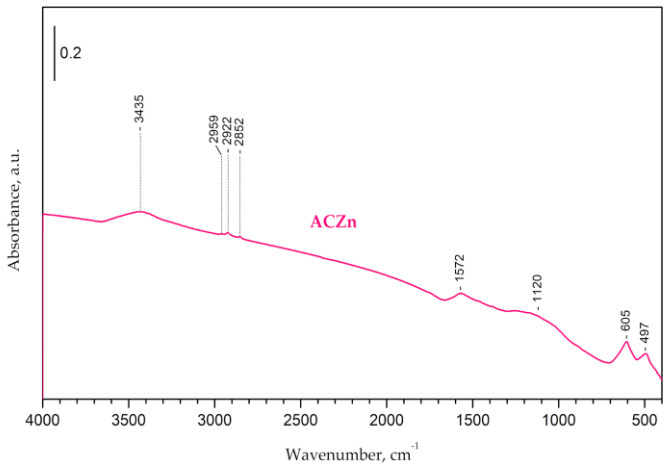

(b)

Фиг. 43 FTIR спектрите на пробите AC и AC18M (а) и ACZn (б)

No significant number of absorption peaks is observed in the FTIR spectra of the ACZn sample, since the material exhibits a high degree of graphitization/ aromatization. However, the

absorption band at 605 cm^{-1} corresponds to the metal–oxygen vibrational mode (Zn–O stretching vibrations). The γ(O–H) band is located at approximately 497 cm^{-1} (Fig. 43b).

The FTIR results indicate the presence of oxygen-containing functional groups on the surface, which enhance the catalytic properties of the functionalized activated carbons. The main oxygen functional groups introduced after functionalization are carbonyl, ether, ester, and hydroxyl (–OH) groups. FTIR and XPS analyses show that acidic surface groups introduced by modification with sulfuric acid and $ZnCl_2$ provide both Lewis and Brønsted active sites. All analyzed samples exhibit similar features in their Raman spectra in the 800–2000 cm^{-1} region, showing the characteristic D and G bands located at approximately 1360 cm^{-1} and 1560 cm^{-1}, respectively, under visible excitation [6, 36].

The sulfonated AC sample shows a reduced Raman signal intensity due to the introduction of $–SO_3H$ groups. The higher content of SO_3H in AC18M increases the degree of oxidation and disrupts the sp^2 domains associated with methylene and phenyl structures.

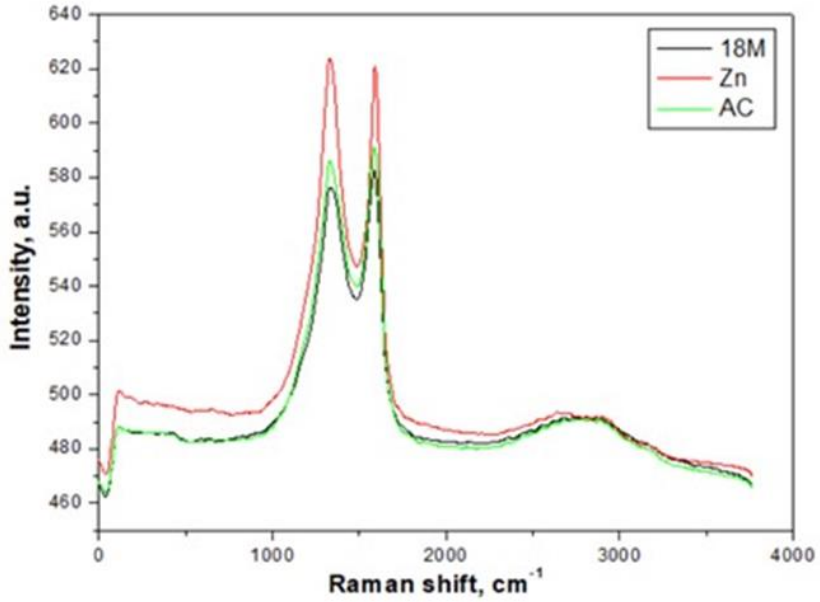

Fig. 44. Raman spectra of activated carbon (AC) from almond shells and catalysts AC18M and ACZn

The Raman spectra of the investigated samples (Fig. 44) show two peaks at approximately 1600 cm^{-1} and 1330 cm^{-1}, corresponding to the G and D bands. The intensity ratio of these bands (I_D/I_G) provides an estimate of the disorder induced by the functionalization process (Table 26). The I_D/I_G ratios for all three samples are close to 1, with the Zn-modified sample being closest to unity. This is expected, since AC and the modified catalysts were obtained by pyrolysis and calcination up to 700 °C, and within this temperature range the I_D/I_G ratio typically does not exceed 1. Sulfuric acid treatment slightly reduces the I_D/I_G ratio of the original AC (Table 26), indicating that the modification increases the structural order.

Table 26. Intensity and D/G band ratio of the investigated samples.

Sample	D (cm-1)	G (cm-1)	ID/IG
AC	1313	1600	0.9922
AC18M	1313	1597	0.9837
ACZn	1327	1597	0.9967

3.4. Synthesis of 5-hydroxymethylfurfural (HMF)

The mechanism of glucose conversion to 5-hydroxymethylfurfural (HMF) begins with glucose activation in an acidic medium. Mineral acids (H_2SO_4, HCl) or acid-modified activated carbons protonate the hydroxyl and carbonyl groups of the molecule, increasing the electrophilicity of the carbon skeleton and facilitating the transition from cyclic to linear form, a necessary step for subsequent dehydration.

In the presence of acidic sites, the protonated linear glucose undergoes water elimination through the formation of short-lived enolic and carbocation intermediates, which prepare the molecule for isomerization. The key step is the isomerization of glucose to fructose, catalyzed by Lewis acids, such as metal sites on the surface of activated carbon. These sites coordinate the carbonyl group and stabilize reactive intermediates, facilitating hydride or hydroxyl group transfer and leading to the formation of fructose, a more dehydration-prone intermediate.

The combination of Lewis and Brønsted acid sites (e.g., ACZn and AC18M) enables simultaneous isomerization and dehydration in a single reactor, thereby increasing both the reaction rate and selectivity. The final step involves triple dehydration of fructose: sequential protonation and elimination of three hydroxyl groups, with the formation of enolic and carbocation intermediates, which rapidly rearrange to form the aromatic furan ring of 5-HMF (Fig. 45).

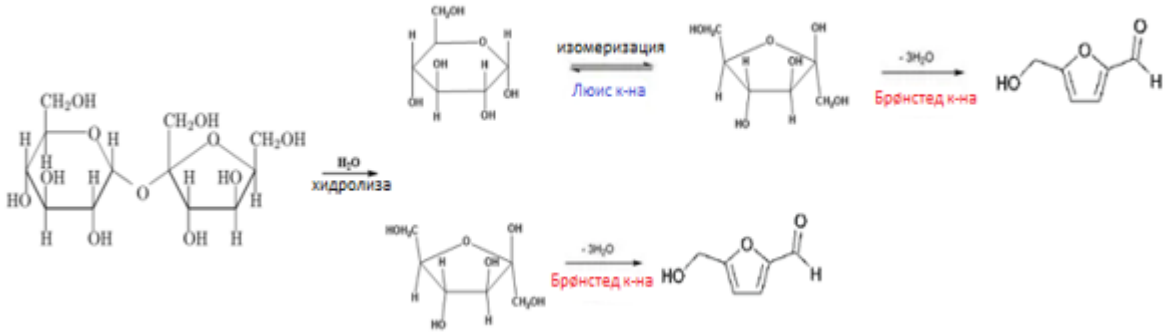

Fig. 45. Reaction scheme for the production of HMF from glucose

In the present dissertation, catalysts functionalized with Lewis and Brønsted acid sites (ACZn, AC18M) were evaluated for the conversion of glucose to HMF in a biphasic water/THF/NaCl system at 160 °C.

The THF/water mixture alone does not catalyze the reaction and acts solely as a solvent (Table 27). The addition of NaCl saturates the aqueous phase and separates THF from water into two distinct layers. It is well known that the use of a biphasic system (THF/water/NaCl) significantly improves HMF extraction compared to monophasic systems. In this system, the formed HMF is extracted in situ into the THF phase, reducing its contact with water and preventing its degradation into undesired by-products such as levulinic acid and formic acid.

A certain amount of HMF may remain in the aqueous phase or be lost due to side reactions, degradation, or incomplete phase separation, as reported in numerous studies on HMF production. The HMF yields reported in this study are based on the amount measured in the organic phase after extraction. Despite minor losses due to incomplete extraction from the aqueous phase, the results show that the experiment conducted without NaCl addition yields only 2.7% HMF. Glucose conversion without a catalyst but in the presence of NaCl results in a 37% HMF yield, while similar trends are observed for reactions catalyzed by sulfuric acid, $ZnCl_2$, and their combination (experiments were carried out using amounts of H_2SO_4 and $ZnCl_2$ corresponding to those in catalysts ACZn and AC18M) (Table 27).

Table 27. HMF yield from glucose conversion using a 50/50 mixture of ACZn and AC18M catalysts

Catalyst	Solvent	Yeld 5-HMF, %
-	THF/water	2.7
-	THF/water/NaCl	37.1
AC	THF/water/NaCl	39.4
ACZn	THF/water/NaCl	55.2
AC18M	THF/water/NaCl	47.9
H2SO4	THF/water/NaCl	36
$ZnCl_2$	THF/water/NaCl	37.6
H2SO4/$ZnCl_2$	THF/water/NaCl	32.2

The glucose yield at the 7th hour at 160 °C reaches 55.2% when using the ACZn catalyst and 47.9% with the AC18M catalyst. These results indicate that both catalysts play an important

role, supporting observations reported by other researchers [12]. Fig. 46 shows the results of HMF production from glucose using the combined AC18M and ACZn catalysts.

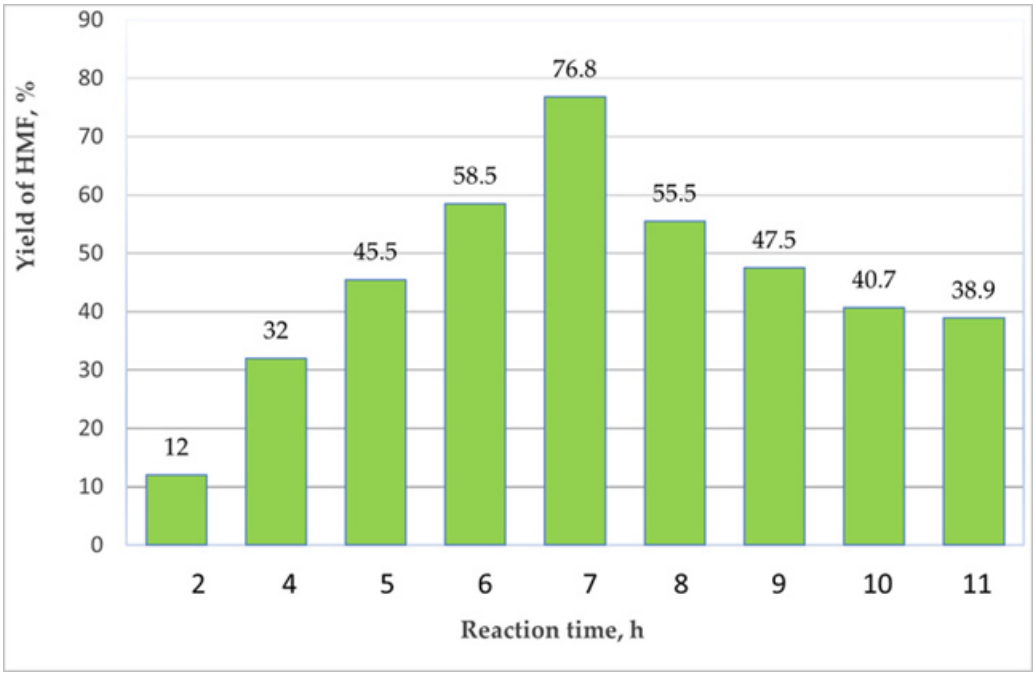

Fig. 46. Conversion of glucose to HMF using a 1:1 mixture of ACZn and AC18M catalysts.

The catalytic efficiency of AC functionalization is confirmed by the yield achieved in HMF production. When using the modified AC catalyst, a high HMF yield of 76.8% was obtained, highlighting the improved performance compared to the non-modified variant. In contrast, the use of non-modified AC as a catalyst results in a significantly lower HMF yield of only 39%, as detailed in Table 24. This almost twofold increase in yield emphasizes the significant influence of surface functional groups on the efficiency of glucose conversion.

In conclusion, catalysts synthesized from sustainable raw materials, specifically almond shells, were developed. The carbonized precursors were functionalized using zinc dichloride or subjected to sulfonation, thereby introducing Lewis acid (LA) or Brønsted acid (BA) sites on their surface. Zn^{2+} ions act as Lewis acids, and their presence was confirmed by PXRD and XPS analyses. BA sites are introduced through sulfonic acid groups ($–SO_3H$) on the carbon surface (confirmed by XPS and FTIR analyses).

The obtained catalytic system demonstrates properties that are critical for enhancing glucose conversion to 5-HMF. The combination of LA and BA active sites in the AC18M and ACZn catalyst mixture improves catalytic efficiency and increases 5-HMF yields.

The analysis shows that these catalysts possess relatively high specific surface area and predominantly microporous structure, while achieving a glucose yield of 76.8%. Therefore, in addition to favorable textural properties, the presence of acidic active sites and oxygen-containing surface groups are significant factors influencing performance. This highlights the

importance of detailed investigation and optimization of chemical activity for further improvement of yields.

CONCLUSIONS

1. Methodologies have been developed for the effective valorization of waste biomass and industrial residues through the production of carbon adsorbents.
2. It has been established that the type of precursor and the activation method determine the porous structure and adsorption properties of the obtained carbon materials.
3. For the first time in this work, a turbostratic carbon material was obtained from polystyrene waste in an open reactor without the application of pressure, characterized by a hierarchical porous structure (micro-, meso-, and macropores). The proposed approach is technologically simple and has potential for scale-up.
4. Activated carbons with a developed micro- and mesoporous structure were obtained from RDF, and samples with good adsorption performance were identified.
5. A microporous adsorbent was obtained from bituminous waterproofing material, showing high efficiency in the removal of organic pollutants, where adsorption behavior depends on the relationship between pore structure and molecular size.
6. For the first time, an energy-efficient method for the synthesis of carbon foam in an open system without pressure and without a stabilization stage was developed, significantly simplifying the process and creating conditions for easy scale-up and practical application. The use of agricultural and industrial waste for producing activated carbons represents a sustainable and environmentally sound approach with potential socio-economic impact.
7. Catalysts based on biomass-derived activated carbon were obtained through targeted chemical modification introducing Brønsted and Lewis acid sites. It was shown that the combination of both types of active sites leads to a pronounced synergistic effect and high efficiency in the conversion of glucose to 5-hydroxymethylfurfural (HMF).

CONTRIBUTIONS

• An integrated approach has been developed for the valorization of various waste raw materials through their conversion into functional carbon materials with controlled structure and properties.

• A relationship has been established between the origin and composition of the precursor materials, processing conditions, and the formation of porous and graphite-like structures that determine the functional properties of the materials.

• A simplified and scalable method has been developed for obtaining turbostratic carbon from polymer waste in an open system without pressure, yielding materials with a high degree of structural ordering and potential for electrochemical and catalytic applications.

• An energy-efficient method for the synthesis of carbon foam has been developed in an open vessel under atmospheric conditions without the use of an inert atmosphere, significantly simplifying the process and creating conditions for industrial application.

• Efficient carbon adsorbents have been produced from various waste sources, and their applicability for the removal of organic pollutants has been demonstrated.

• Heterogeneous carbon catalysts with combined Brønsted and Lewis acid sites have been developed, for which a synergistic effect in the conversion of glucose to 5-hydroxymethylfurfural has been established.

Publications indexed in Scopus and Web of Science databases.

1. Stoycheva, I., Tsyntsarski, B., Vasileva, M., Petrova, B., Georgiev, G., Budinova, T., Szeluga, U., Pusz, S., Kosateva, A., Petrov, N. New method for synthesis of carbon foam on the base of mixture of coal tar pitch and furfural without using pressure and stabilization treatment. Diamond and Related Materials, 109, Elsevier, 2020, ISSN:0925-9635, 1-8, https://doi.org/10.1016/j.diamond.2020.108066
2. Tsyntsarski, B., Toteva, VB, Nickolov, RN, Banchev, I, Stoycheva, I, Gonsalvesh, L, Petrova, B, Georgiev, G, Vasileva, M, T. Budinova, Petrov, N. Conversion of waste algae from biodiesel production to valuable gas, liquid and solid products. Journal of Material Cycles and Waste Management, 22, Springer, 2020, 1176-1183 https://doi.org/10.1007/s10163-020-01010-9
3. Georgiev, G., Tsyntsarski, B., Stoycheva, I., Kosateva, A., Petrova, B., Miteva, K., Budinova, T., Petrov, N., Sarbu, A., Dumitru, M., Ciurluca, A., Miron, A.. Refuse-derived fuel waste conversion to carbon adsorbent. Bulgarian Chemical Communications, 53, Special Issue A, Bulgarian Academy of Sciences, 2021, 89-92 https://doi.org/10.34049/bcc.53
4. Firas Feki, F., Tsyntsarski, B., Sayadi, S., Georgiev, G., Dimitrov, V.. Adsorption capacity, structure and surface properties of activated carbons produced from pistacia lentiscus by-product. Surveying

Geology and Mining Ecology Management, 4, SGEM, 2021, 19-23 https://doi.org/10.5593/sgem2021/4.1/s17.03

5. Stoycheva, I., Tsyntsarski, B., Kosateva, A., Petrova, B., Georgiev, G., Miteva, K.. Activated carbon foam derived from treatment products of rdf without pressure and stabilization stage for removal of pollutants from water. Comptes Rendus de l'Academie Bulgare des Sciences, 75, 2, БАН, 2022, 216-222, https://doi.org/10.7546/CRABS.2022.02.06.

6. Toteva, V.; Georgiev, G.; Angelova, D.; Godzierz, M. Tailored Carbon Catalysts Derived from Biomass for Efficient Glucose-to-5-ХМФ Transformation. Sustainability 2026, 18, 1254. https://doi.org/10.3390/su18031254.